6. REFERENCES:

Andersen, N. J. B. and Ainslie, L. C, 1994. Neotectonic reactivation – an aid to the location of groundwater. African Geoscience Review 1 (no.1): 1-10.

Anderson, E. M. 1951. *The dynamics of faulting and dyke formation with applications to Britain*. Edinburgh: Oliver & Boyd. 206 p.

Andreoli, M. A. G., M. Doucoure, J. Van Bever Donker, D. Brandt, and N. J. B. Andersen 1996. Neotectonics of southern Africa: A review. Africa Geosc. Rev. 3 (no.1): 1-16.

Anhaeusser, C.R. 1992. Structures in granitoid gneisses and associated migmatites close to the boundary of the Limpopo Belt, South Africa. Precambrian Res., 55: 81-92.

Aydin, A. 1978. Small faults formed as deformation bands in sandstone. Pure and Applied Geophysics. 116: 913-930.

Aydin, A. and Johnson, A. M., 1978. Development of faults as zones of deformation bands and as slip surfaces in sandstone. Pure and Applied Geophysics. 116: 931-942.

Barker, O.B. 1979. "A contribution to the geology of the Soutpansberg Group, Waterberg Supergroup, northern Transvaal." Unpublished M.Sc. thesis, University of the Witwatersrand, Johannesburg.

Barker, O. B., 1983. A proposed geotectonic model for the Soutpansberg Group within the Limpopo Mobile Belt, South Africa. Special Publication of the Geological Society of South Africa. 8: 181-190.

Barker, O. B., Brandl, G., Callaghan, C. C., Eriksson P. G. and Van der Neut, M. 2006. The Soutpansberg and Waterberg Groups and the Blouberg Formation. *In:* Johnson, M. R. (Ed.), *The geology of South Africa.* Pretoria: The Geological Society of South Africa and the Council for Geoscience.

Barton, J.M., Robb, L.J., Anhaeusser, C.R. and van Nierop, D.A. 1983. Geochronologic and Sr-isotopic studies of certain units in the Barberton granite-greenstone terrane, South Africa. *In*: Anhaeusser, C.R. (Ed.), *Contributions to the geology of the Barberton Mountainland*. Spec. Publ. Geol. Soc. S. Afr. 9: 6-72.

Barton Jr., J. M., Van Reenen, D.D., Roering, C.A. 1990. The significance of 3000 Ma granulite facies mafic dykes in the central zone of the Limpopo belt, southern Africa. Precamb. Res., 48: 299-308.

Barton, J.M., Doig, R., Smith, C.B., Bohelnder, F. and van Reenen, D.D. 1992. Isotopic and REE characteristics of the intrusive charnoenderbite and enderbite geographically associated with the Matok Pluton, Limpopo Belt, southern Africa. Precambrian Res., 55: 451-467.

Barton Jr., J.M., Pretorius, W. 1997. Soutpansberg age (1.85 Ga.) magmatism and metallogenesis in southern Africa: a result of regional rifting. Abstract: International Symposium on Plumes, Plates and Mineralization. University of Pretoria, South Africa.

Bird, P., Ben-Avraham, Z., Schubert, G., Andreoli, M., and Viola, G. 2006. Patterns of stress and strain rate in southern Africa. Journal of Geophysical Research 111, B08402.

Bohlender, F. 1992. "Igneous and metamorphic charnockitic rocks in the Southern Marginal Zone of the Limpopo Belt with special emphasis on the Matok enderbitic-granitic suite." Unpublished Ph.D. thesis, Rand Afrikaans University, Johannesburg, 261pp.

Bosch, P.J.A. (1992). "Die Geologie van die Wolkberg Groep tussen die Abel Erasmuspas en Graskop, Oos Transvaal." Unpublished M.Sc. thesis, University of Pretoria, South Africa, 290pp.

Brandl, G. (1985). Sheet 2328 Pietersburg (1:250000 Geological series). Geol Surv. S. Afr.

Brandl, G. (1986). The geology of the Pietersburg area. Explanation of sheet 2328 (1:250000 Geological series) Geol Surv. S. Afr., 43pp.

Brandl, G., 1987. The geology of the Tzaneen area. Explanation of sheet 2330. Geol. Surv. S. Afr., Pretoria 43 pp.

Brandl, G. (1987). The geology of the Tzaneen area. Explanation of Sheet 2330 (1:250000 Geological series) Geol Surv. S. Afr., 55pp.

Brandl, G. and Kröner, A. 1993. Preliminary results from single zircon studies from various Archaean rocks of the north-eastern Transvaal. Abstr. 16th Coll. African geology, Mbabane, Swaziland. 1: 54-56.

Brandl, G. 1995. Reactivation of certain faults in the Limpopo Belt during the Quaternary. *In* Extended Abstracts of the Centennial Geocongress, vol. 1, J. M. Barton and Y. E. Copperthwaite, pp. 442– 444, Geol. Soc. of S. Africa, Johannesburg.

Brandl, G., Jaeckel, P. and Kröner, A. (1996). Single zircon age for the felsic Rubbervale Formation, Murchison greenstone belt, South Africa. S. Afr. J. Geol., 99, 229-234.

Brandl, G. (in press). Mashashane Suite, including the Lunsklip, Uitloop and Uitvlught granite. In: Johnson, M.R. (Ed.), Catalogue of South African Lithostratigraphic Units. S. Afr. Comm. Strat.
Bromley, J. Mannström, B., Nisca, D. and Jamtlid, A. (1994). Airborne geophysics: application to ground-water study in Botswana. Ground Water, 32. 79-90.

Bumby, A.J., 2000. "The geology of the Blouberg Formation. Waterberg and Soutpansberg Groups in the area of Blouberg mountain, Northern Province, South Africa." Unpublished Ph.D. thesis, University of Pretoria, South Africa.

Bumby, A.J., Eriksson, P.G., van der Merwe, R., Maier, W.D., 2001. The stratigraphic relationship between the Waterberg Group and the Soutpansberg Group (Northern Province, South Africa): Evidence from the Blouberg area. S. Afr. J. Geol. 104 (3).

Bumby, A.J., et al. 2002. A half-graben setting for the Proterozoic Soutpansberg Group (South Africa): evidence from the Blouberg area. Sedimentary Geology 147: 37-56.

Bumby, A.J., et al. 2004. The early Proterozoic sedimentary record in the Blouberg area, Limpopo Province, South Africa; implications for the timing of the Limpopo orogenic event. Journal of African Earth Sciences 39: 123-131.

Burke, K. & Dewey, J.F. 1973. Plume-generated triple junctions: key indicators in applying plate tectonics to old rocks. J. Geol., 81: 406-433.

Button, A. 1973. A study of the stratigraphy and development of the Transvaal basin in the eastern and northeastern Transvaal. Unpublished Ph. D. thesis, University of the Witwatersrand, Johannesburg, 133pp.

Byerlee, J. D. 1967. Frictional characteristics of granite under high confining pressure. Journal of Geophysical Research 72: 3639-3648.

Byerlee, J. D. 1978. Friction of Rocks. Pure and Applied Geophysics 116: 615-626.

Cheney, E.S., Barton Jr., J.M., Brandl, G. 1990. Extent and age of the Soutpansberg sequences of southern Africa. S. Afr. J. Geol. 93: 644– 675.

Cook, P.G. 2003. A guide to regional groundwater flow in rock aquifers. CSIRO, Australia. 108 pp.

Coulomb, C. A. 1773. Sur une application des regles de maximus et minimis a quelques ploblemes de statique relatives a l'architecture: Academie Royale des Sciences, Memoires de Mathematique de Physique par divers Savants. 7: 343-382.

Cox, K. G. 1992. Karoo igneous activity and the early stages of break-up of Gondwanaland. *In: Magmatism and the causes of continental breakup*. Sotey, B. C., Alabaster, A. And Pankhurst, R. J. (eds.). Geological Society of London Special Publication.

Davis, G. H. and Reynolds, S. J. 1996. Structural geology of rocks and regions. Second edition: Wiley & Sons, New York.

The Municipal Demarcation Board of South Africa (cited Nov. 10, 2008).
Available at: www.demarcation.org.za

De Villiers, S.B. and Brandl, G. 1977. Die Mashashane granietplutoon noordoos van Potgietersrus. Ann. Geol, Surv. S. Afr., 11: 7-13.

De Wit, M. J., et al. 1992. Formation of an Archaean continent. Nature 357: 553-562.

De Wit, M. J., et al., 1993. Gold-bearing sediments in the Pietersburg greenstone belt: age equivalents of the Witwatersrand Supergroup sediments, South Africa. Econ. Geol. 88: 1242-1252.

Donath, F. A., 1961. Experimental study of shear failure in anisotropic rocks: Geological Society of America Bulletin 72: 985-989.

Government Communication and Information System (GCIS) 2004. South Africa Yearbook 2003/04. Pretoria: GCIS and STE Publishers. ISBN 1-919855-18-1. Available: http://www.gcis.gov.za/docs/ publications/yearbook.htm [2008, 7 November]

Grantham, G. H. 1996. Aspects of Jurassic Magmatism and Faulting in western Dronning Maud Land, Antarctica: Implications for Gondwana breakup. pp. 63-71 in *Weddell Sea Tectonics and Gondwana Break-up*. Sorey, B. C., King, E. C. and Livingstone, R. A. (Eds.). Geological Society Special Publication No. 108.

Groundwater Resources Information Project, 2002. Department of Water Affairs and Forestry of South Africa.

Hafner, W. 1951. Stress distribution and faulting. Geological Society of America Bulletin 62: 373-398.

Hatton, C. J. 1995. Primary magmas in the Ventersdorp and Bushveld Igneous Provinces: Magma extraction from a lower mantle plume. *Ext. Abstr. Centennial Geocongress,* Geol. Soc. S. Afr., Rand Afrikaans Univ. 1, 520-521.

Handin, J. 1969. On the Coulomb-Mohr failure criterion. Journal of Geophysical Research 74: 5343-5348.

Hartnady, C. J. H. 2002. Earthquake hazard in Africa: Perspectives on the Nubia-Somalia boundary, S. Afr. J. Sci. 98: 425– 428.

Henderson, D.R., Long, L.E. and Barton, J.M. 2000. Isotopic ages and chemical and isotopic composition of the Archaean Turfloop batholith, Pietersburg granite-greenstone terrane, Kaapvaal Craton, South Africa. S. Afr. J. Geol. 103: 38-46.

Holzer, L., Frei, R., Barton, Jr., J.M., Kramers, J.D. 1998. Unravelling the record of successive high grade events in the Central Zone of the Limpopo belt using Pb single phase dating of metamorphic minerals. Precambrian Res. 83: 87-115.

Horton, G. A., 1999. *Water Words Dictionary*. Nevada Division of Water Planning, Department of Conservation and Natural Resources, Nevada.

Hubbert, M. K., and Rubey, W. W. 1959. Role of fluid pressure in mechanics of overthrust faulting. Part 1: Geological Society of America Bulletin 70: 115-166.

Jansen, H. 1975. The Soutpansberg Trough – An Aulocagen. Transactions of the Geological Society of South Africa 78: 129-136.

Klein, J. A. 1980. Pleistocene to Recent faulting in the area west of Omaruru (SWA/Namibia). Reg. Geol. Ser. Open File Rep. RG-4, 28 pp., Geol. Surv. of Namibia, Windhoek.

Kröner, A., Jaeckel, P., Brandl, G. 2000. Single zircon ages for felsic to intermediate rocks from the Pietersburg and Giyani greenstone belts and bordering granitoid orogneisses, northern Kaapvaal Craton, South Africa. J. Afr. Earth Sci. 30 (no.4): 773-793.

McCarthy, T. S., N. D. Smith, W. N. Ellery and T. Gumbricht 2002. The Okavango delta: Semiarid alluvial-fan sedimentation related to incipient rifting, in Sedimentation in Continental Rifts, Spec. Publ. SEPM Soc. Sediment. Geol. 73: 179– 193.

McCourt, S., Armstrong, R.A., 1998. SHRIMP U-Pb zircon chronology of granites from the Central Zone, Limpopo Belt, southern Africa: implications for the age of the Limpopo Orogeny. S. Afr. J. Geol. 101: 329-337.

Mohr, O. C., 1990. Welche Umstande bedingen die Elastizitatsgrenze und den Bruch eines Materials: Zeitschrift der Vereines Deutscher Ingenieure 44: 1524-1530 and 1572-1577.

Mulwa, J., Gaciri, S., Barongo, J., Opiyo-Akech, N. and K., 2005. Geological and structural influence on groundwater distribution and flow in Ngong area, Kenya. African Journal of Science and Technology, Science and Engineering Series, V. 6, No. 1: 105-115.

Partridge, T. C. and R. R. Maude 2000. Macro-scale geomorphic evolution of southern Africa, in The Cenozoic of Southern Africa, Oxford Monogr. Geol. Geophys. 40: 3-18. Oxford Univ. Press, New York. (edited by T. C. Partridge and R. R. Maude)

Perchuk, L. L., Gerya, T. V., Van Reenen, D. D., Smit, C. A. and Krotov, A. V., 2000. P-T paths and tectonic evolution of shear zones separating high-grade terrains from cratons: examples from the Kola Peninsula (Russia) and the Limpopo Region (South Africa). Mineralogy and Petrology. 69: 109-142.

Poujol, M., Robb, L.J., Respaut, J.P., Anhaeusser, C.R. 1996. 3.07-2.97 Ga. greenstone belt formation in the northeastern Kaapvaal Craton: Implications for the origin of the Witwatersrand Basin. Econ. Geol. 91 (no.8): 1455-1461.

Poujol, M. and Robb, L.J. 1999. New U-Pb zircon ages on gneisses and pegmatite from south of the Murchison greenstone belt, South Africa. S. Afr. J. Geol. 102: 93-97.

Poujol, M. 2001. U-Pb isotopic evidence for episodic granitoid emplacement in the Murchison greenstone belt, South Africa. J. Afr. Earth Sci. 33: 155-163.

Poujol, M., Robb, L.J., Anhaeusser, C.R. and Gericke, B. 2003. A review of the geochronological constraints on the evolution of the Kaapvaal Craton, South Africa. Precambrian Research 127: 181-213.

Reches, Z. 1978. Analysis of faulting in a three-dimensional strain field: Tectonophysics 47: 109-129.

Reches, Z. 1983. Faulting of rocks in three-dimensional strain fields: 1. Failure of rocks in polyaxial, servo-control experiments: Tectonophysics 95: 111-132.

Robb, L.J. 1978. A general geological description of the Archaean granitic terrane between Nelspruit and Bushbuckridge, eastern Transvaal. Trans. Geol. Soc. S. Afr. 81: 331-338.

Robb, L.J. 1994. Cunning Moor Tonalite. *In*: Johnson, M.R. (Ed.) *Catalogue of South African Lithostratigraphic Units*. S. Afr. Comm. Strat. 5-11, 5-12.

Robb, L.J., Brandl, G., Anhaeusser, C.R. and Poujol, M. 2006. Arachaean Granitoid Intrusions. *In*: Johnson, M.R., Anhaeusser, C.R. and Thomas, R.J. (Eds.) *The Geology of South Africa*. Geological Society of South Africa, Johannesburg/Council for Geoscience, Pretoria 57-94.

Sami, K., Neumann, I., Gqiba, D., De Kock, G. and Grantham, G. 2002. Groundwater exploration in geologically complex and problematic terrain: Limpopo Mobile Belt. Water Research Commission Report, v. 2, chp.3.

Sanford, A. R. 1959. Analytical and experimental study of simple geologic structures: Geological Society of America Bulletin 70: 19-52.

Schaller, M. et al. 1999. Exhumation of Limpopo Central Zone granulites and dextral continent-scale transcurrent movement at 2.0Ga. along the Palala Shear Zone, Northern Province, South Africa. Precambrian Res. 96: 263-288.

Secor, D. T. 1965. Role of fluid pressure in jointing: American Journal of Science 263: 633-646.

Smit, C. A., Roering, C. and Van Reenen, D. D., 1992. The structural framework of the northern margin of the Limpopo Belt, South Africa. Precambrian Research. 55: 51-67.

Statistics South Africa 1998. The people of South Africa, Population Census, 1996: Census in Brief. Report No. 1: 03-01-11 (1996). Pretoria: Statistics South Africa.

SSA (2002a). *Income and Expenditure Survey 2000,* Pretoria: Statistics South Africa.

SSA (2002b). *Labour Force Survey September 2000,* Pretoria: Statistics South Africa.

SSA (2003a). *Census 2001,* Pretoria: Statistics South Africa.

Statistics South Africa. 2003. Census 2001: Census in Brief. Report No. 03-02-03 (2001). Pretoria: Statistics South Africa.

Stacey, T. R., and J. Wesseloo 1998. Final Project Report: Evaluation and upgrading of records of stress measurement data in the mining industry, GAP 511b, 31 pp. + appendices, Safety in Mines Res. Adv. Comm. (SIMRAC), Johannesburg.

Stettler, E.H., de Beer, J.H. and Blom, M.P. 1989. Crustal domains in the northern Kaapvaal as defined by magnetic lineaments. Precambrian Res. 45: 263-276.

Suppe, J., 1985. *Principles of structural geology*. Prentice-Hall: Englewood Cliffs, New Jersey, 537p.

Twiss, R. J., and Moores, E. M. 1992. *Structural geology*. New York: W. H. Freeman & Company, 532p.

Uken, R., Watkeys, M.K. 1997. An interpretation of mafic dyke swarms and their relationship with major mafic magmatic events on the Kaapvaal Craton and Limpopo Belt. S. Afr. J. Geol. 100 (no.4): 341-348.

University of Idaho's Glossary of Hydrogeology Terms.
Available from: http://www.if.uidaho.edu/~johnson/ifiwrri/sr3/gloss.html.

Van Eeden, O.R., Partridge, F.C., Kent, L.E. and Brandt, J.W. 1939. The mineral deposits of the Murchison range east of Leydsdorp. Mem. Geol. Surv. S. Afr. 36: 172pp.

Vearncombe, J.R., Barton, J.M., Cheshire, P.E., de Beer, J.H., Stettler, E.H. and Brandl, G. 1992. Geology, geophysics and mineralization of the Murchison Schist belt, Rooiwater Complex and surrounding granitoids. Mem. Geol. Surv. S. Afr. 81: 139pp.

Viola, G., M. Andreoli, Z. Ben-Avraham, I. Stengel, and M. Reshef 2005. Offshore mud volcanoes and onland faulting in southwestern Africa: Neotectonic implications and constraints on the regional stress field, Earth Planet. Sci. Lett., 231: 147–160.

Vorster, C.J. 1979. Die geologie van die Klein Letabagebied, noordoos Transvaal, met spesiale verwysing na die granietiese gesteentes. Unpublished M.Sc thesis. Rand Afrikaans Univ., Johannesburg 138pp.

Walraven, F. 1989. The geology of the Pilgrim's Rest area. Explanation of Sheet 2430 (1:250000) Geol. Surv. S. Afr., 24pp.

Wikipedia (modified Aug. 28, 2008; cited Dec. 3, 2008). Tm. Wikipedia Foundation Inc., U.S. registered 501(c)(3) tax-deductible nonprofit charity. Inverse distance weighting. Available from: http:/en.wikipedia.org/wiki/Inverse_distance_weighting

Willmitzer, H. (cited Oct. 15, 2008). Available from:
http://www.waterquality.de/hydrobio.hw/XYZTERMS.HTM

Zoback, M. L., and M. D. Zoback 1989. Tectonic stress field of the continental United States. Mem. Geol. Soc. Am. 172: 523– 539.

7. APPENDIX:

i.

Table 6: A table containing the coordinates for all the waypoints recorded in the field in decimal degrees.

Waypoint	Latitude	Longitude	Waypoint	Latitude	Longitude
1	-23.859917	29.199417	36	-23.2586	28.86785
2	-23.859850	29.188900	37	-23.2661	28.86938
3	-23.875550	29.106550	38	-23.2668	28.87483
4	-23.876733	29.107550	39	-23.2652	28.87315
5	-23.878267	29.109117	40	-23.2682	28.87362
6	-23.883800	29.116100	41	-23.2659	28.86957
7	-23.810050	29.215600	42	-23.2671	28.87025
8	-23.779533	29.158550	43	-23.2738	28.8685
9	-23.782517	29.158233	44	-23.2743	28.86915
10	-23.797417	29.145133	45	-23.2751	28.8718
11	-23.795933	29.149917	46	-23.2755	28.87248
12	-23.792533	29.127583	47	-23.2782	28.86103
13	-23.302867	29.054250	48	-23.2236	28.93787
14	-23.301033	29.055183	49	-23.6371	30.14962
15	-23.515233	29.353417	50	-23.6636	30.1652
16	-23.510683	29.355133	51	-23.5987	30.19453
17	-23.510433	29.355283	52	-23.4836	30.16018
18	-23.745950	29.271083	53	-23.4835	30.16018
19	-23.737683	29.262600	54	-23.551	30.09645
20	-23.688817	29.176383	55	-23.5579	30.09725
21	-23.626733	29.288500	56	-23.555	30.08915
22	-23.791833	29.124950	57	-23.5528	30.09513
23	-23.791500	29.118533	58	-23.5604	30.09147
24	-23.791200	29.117517	59	-23.5339	30.10513
25	-23.788833	29.116100	60	-23.5002	30.14985
26	-23.785917	29.114200	61	-23.5031	30.14532
27	-23.784383	29.111550	62	-23.5189	30.04257
28	-23.486617	28.681667	63	-23.5166	30.04402

Waypoint	Latitude	Longitude	Waypoint	Latitude	Longitude
29	-23.20175	28.72478	60	-23.50015	30.14985
30	-23.21578	28.75555	61	-23.50312	30.14532
31	-23.23052	28.77955	62	-23.5189	30.04257
32	-23.249	28.79877	63	-23.51657	30.04402
33	-23.25727	28.81843	64	-23.5123	29.9966
34	-23.25608	28.86162	65	-22.99323	29.92943
35	-23.25002	28.85835	66	-22.96868	29.94395
36	-23.25857	28.86785	67	-22.92753	29.932
37	-23.26605	28.86938	68	-23.18855	30.08773
38	-23.2668	28.87483	69	-23.61493	29.96477
39	-23.26523	28.87315	70	-23.6047	30.00608
40	-23.26815	28.87362	71	-23.71718	30.15205
41	-23.26588	28.86957	72	-23.78613	30.29683
42	-23.2671	28.87025	73	-23.8017	30.27332
43	-23.27375	28.8685	74	-23.8021	30.2656
44	-23.27425	28.86915	75	-23.75247	30.11002
45	-23.27508	28.8718	76	-23.6326	30.08468
46	-23.27547	28.87248	77	-23.64832	30.08172
47	-23.2782	28.86103	78	-23.64767	30.0884
48	-23.22363	28.93787	79	-23.64835	30.08867
49	-23.63707	30.14962	80	-23.64932	30.0926
50	-23.66358	30.1652	81	-23.6514	30.09363
51	-23.59873	30.19453	82	-23.65213	30.09472
52	-23.48355	30.16018	83	-23.51928	29.49438
53	-23.48352	30.16018	84	-23.5191	29.49503
54	-23.551	30.09645	85	-23.519	29.49538
55	-23.55785	30.09725	86	-23.51887	29.4959
56	-23.55498	30.08915	87	-23.51792	29.49912
57	-23.55275	30.09513	88	-23.48137	29.52992
58	-23.56042	30.09147	89	-23.42985	29.56173

Waypoint	Latitude	Longitude	Waypoint	Latitude	Longitude
59	-23.5339	30.10513	90	-23.44517	29.5862
91	-23.46707	29.63355	122	-23.4769	29.14792
92	-23.47063	29.63482	123	-23.4947	29.19627
93	-23.47315	29.63575	124	-23.5111	29.25137
94	-23.29685	29.5469	125	-23.463	29.29023
95	-23.52085	29.64022	126	-23.4663	29.23182
96	-23.52005	29.64218	127	-23.4896	29.21462
97	-23.51702	29.64487	128	-23.5816	28.77537
98	-23.51567	29.64465	129	-23.5422	28.71507
99	-23.51257	29.64297	130	-23.7513	28.70443
100	-23.51008	29.6416	131	-23.5688	29.88088
101	-23.5056	29.6432	132	-23.5688	29.88088
102	-23.4374	29.44268	133	-23.5057	29.73122
103	-23.52172	29.35575	134	-23.5057	29.7312
104	-23.7277	29.40645	135	-23.5529	29.82422
105	-23.79685	29.35245	136	-23.6104	29.89075
106	-23.76512	29.30138	137	-23.5875	29.88523
107	-23.62653	29.28267	138	-23.555	29.88493
108	-23.61642	29.19882	139	-23.5255	29.90265
109	-23.67662	29.25878	140	-23.5256	29.90265
110	-23.6742	29.28118	141	-23.4506	29.90068
111	-23.66727	29.29983	142	-23.367	30.53257
112	-23.71253	29.27752	143	-23.4471	30.36273
113	-23.5451	29.11297	144	-23.4674	30.30353
114	-23.50502	29.06215	145	-23.4769	30.25368
115	-23.49067	28.99825	146	-23.4924	30.23017
116	-23.4998	28.9782	147	-23.5385	29.7192
117	-23.51298	28.92433	148	-23.5569	29.75663
118	-23.49335	28.91985	149	-23.5203	29.70848
119	-23.41987	28.88787	150	-23.5107	29.66693

Waypoint	Latitude	Longitude
120	-23.39633	28.9282
121	-23.41608	28.99165
166	-23.39977	30.12642
167	-23.50868	30.22278
168	-23.44255	30.15492
169	-23.41923	30.15883
170	-23.41753	30.15207
171	-23.39977	30.12642
172	-23.41672	30.24478
173	-23.41665	30.2444
174	-23.4164	30.24317
175	-23.41557	30.24307
176	-23.41382	30.24138
177	-23.418	30.24282
178	-23.41492	30.19688
164	-23.4013	30.13197
165	-23.3999	30.1262

ii. Poles to planes of joints in each 10’ x 10’ block:

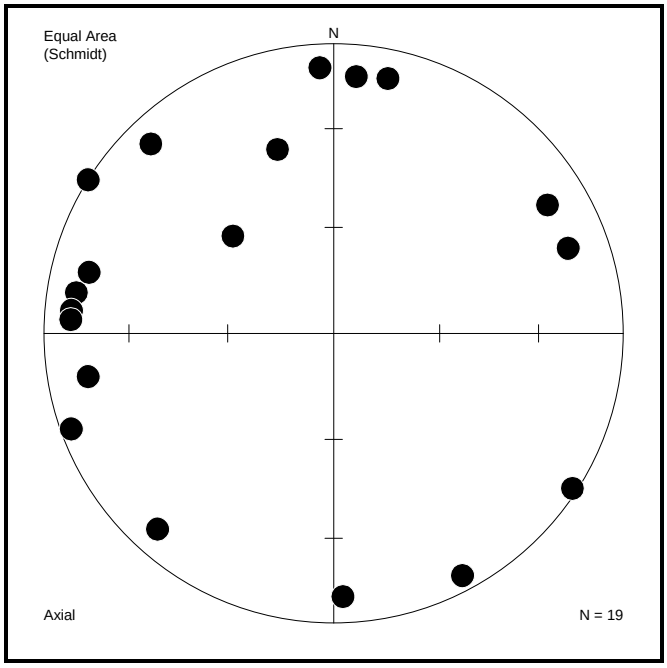

Figure 61: A summary of the poles to joint planes found in block S22° 50’ E29° 50’.

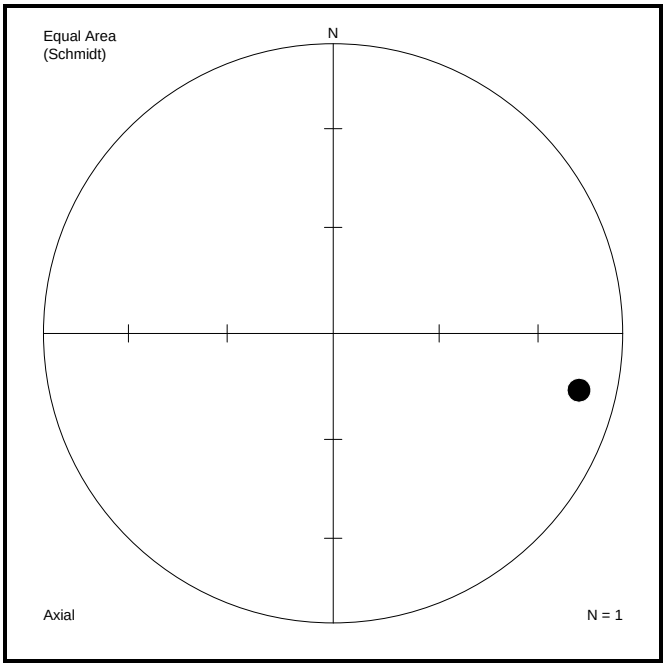

Figure 62: A summary of the poles to joint planes found in block S23° 10’ E29° 00’.

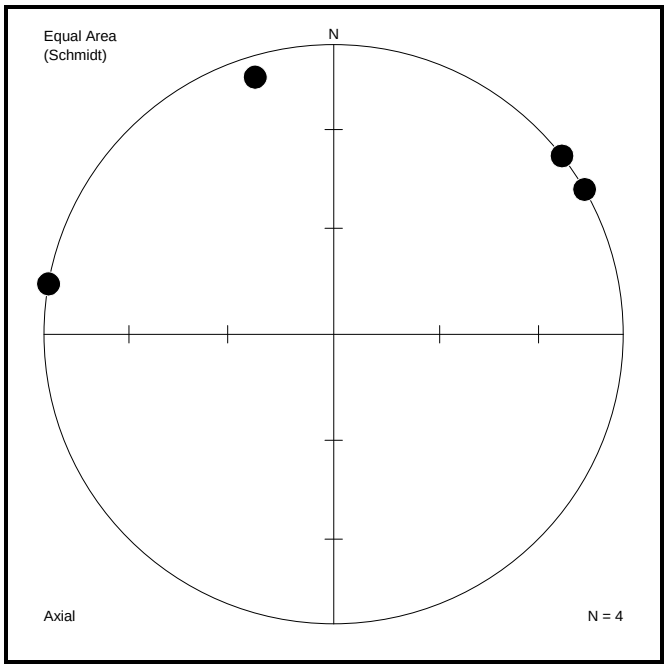

Figure 63: A summary of the poles to joint planes found in block S23° 10’ E29° 30’.

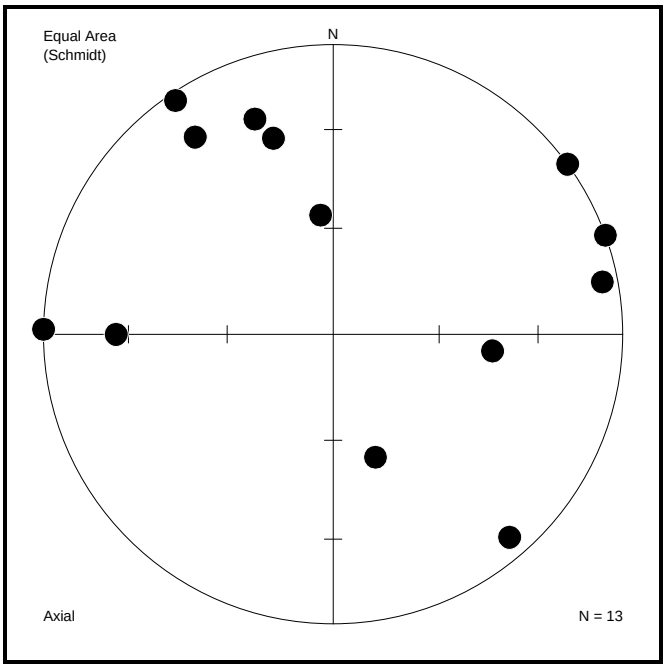

Figure 64: A summary of the poles to joint planes found in block S23° 10’ E30° 00’.

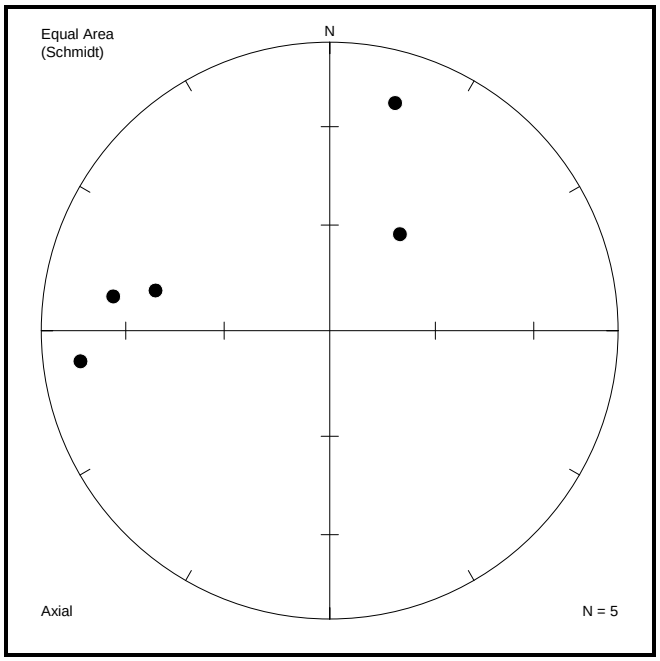

Figure 65: A summary of the poles to joint planes found in block S23° 20' E28° 50'.

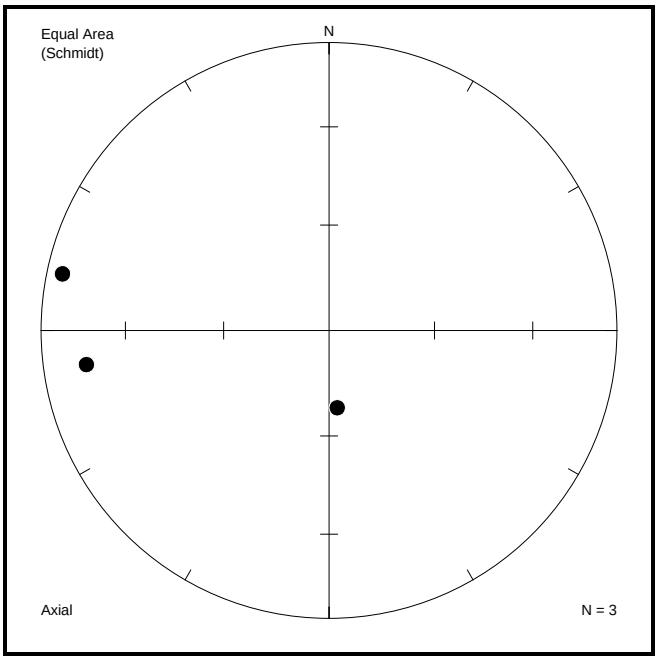

Figure 66: A summary of the poles to joint planes found in block S23° 20' E29° 00'.

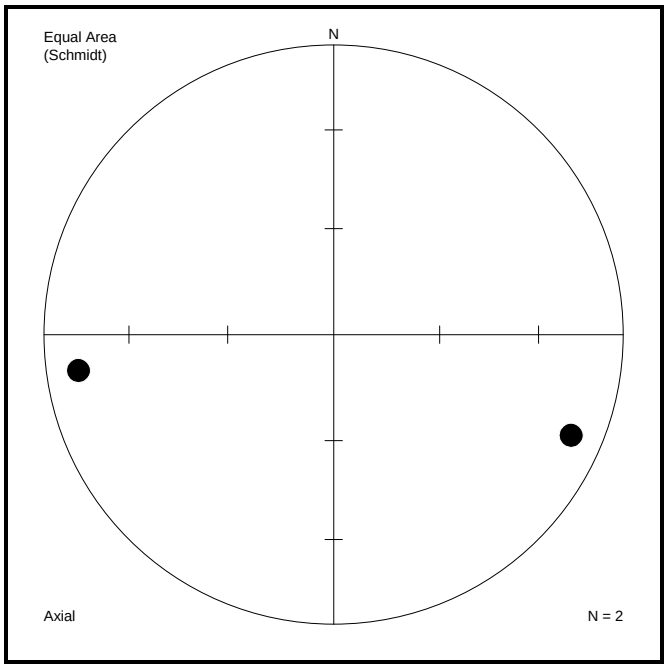

Figure 67: A summary of the poles to joint planes found in block S23° 20' E29° 10'.

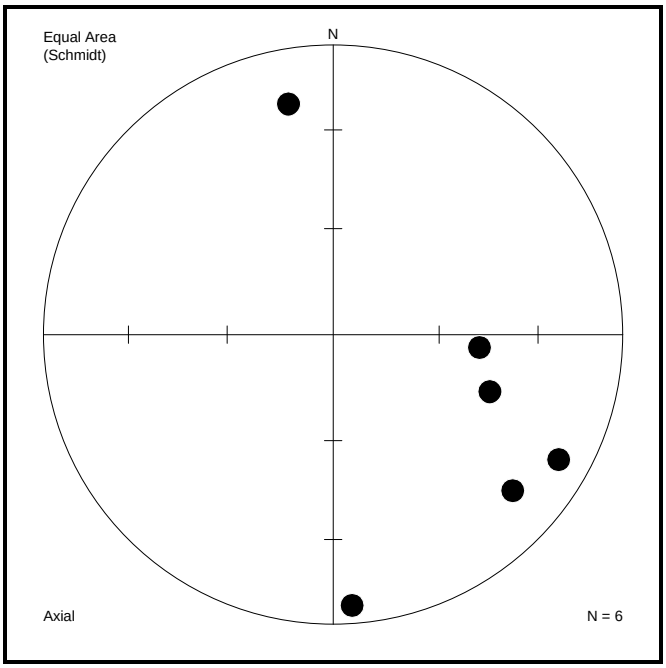

Figure 68: A summary of the poles to joint planes found in block S23° 20' E29° 20'.

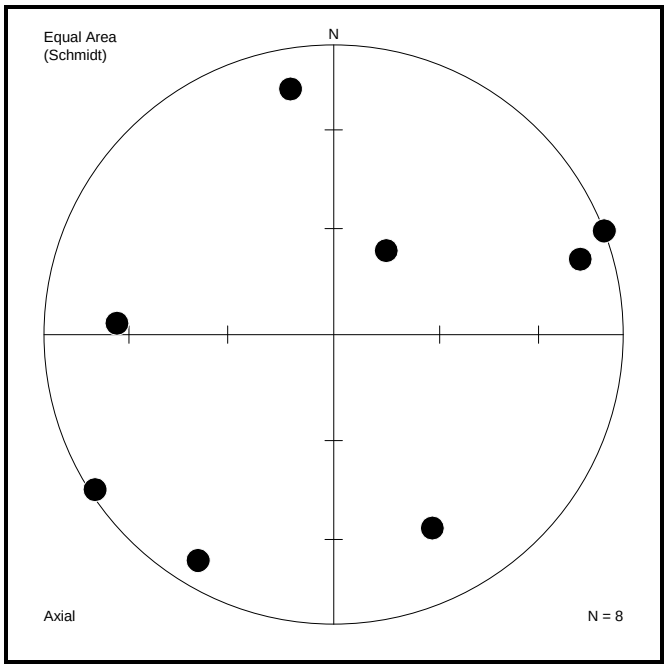

Figure 69: A summary of the poles to joint planes found in block S23° 20' E29° 30'.

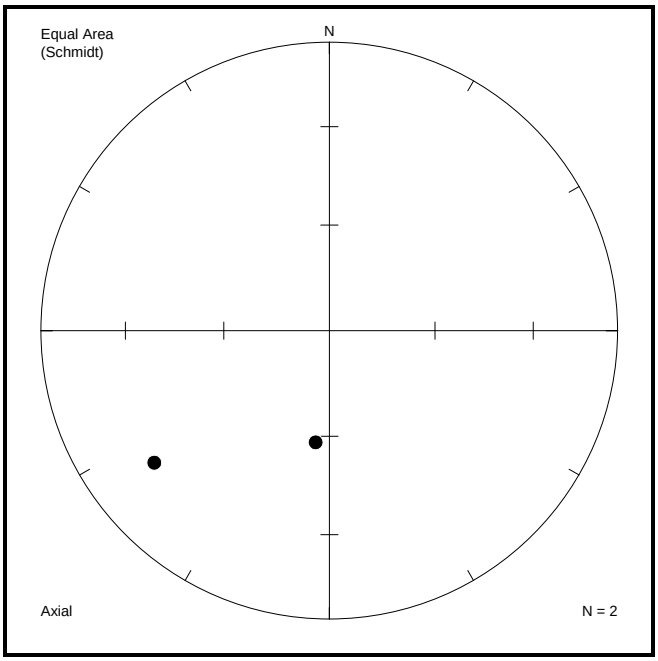

Figure 70: A summary of the poles to joint planes found in block S23° 20' E29° 50'.

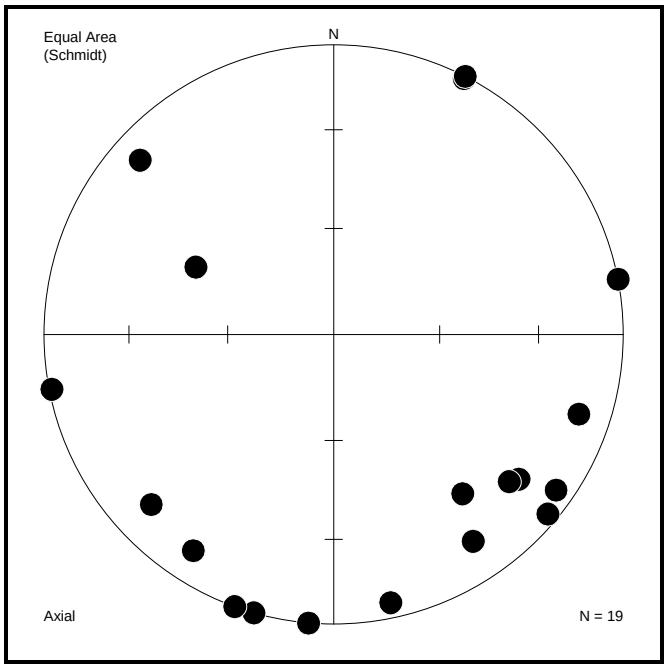

Figure 71: A summary of the poles to joint planes found in block S23° 20' E30° 00'.

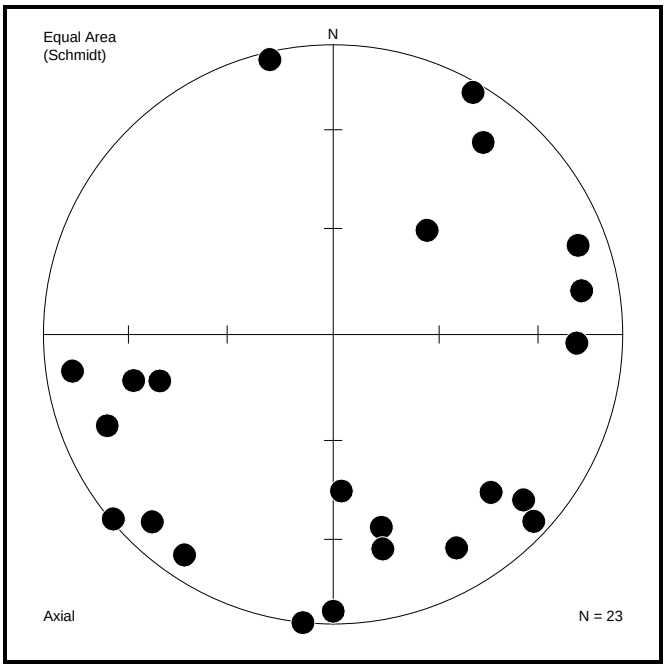

Figure 72: A summary of the poles to joint planes found in block S23° 20' E30° 10'.

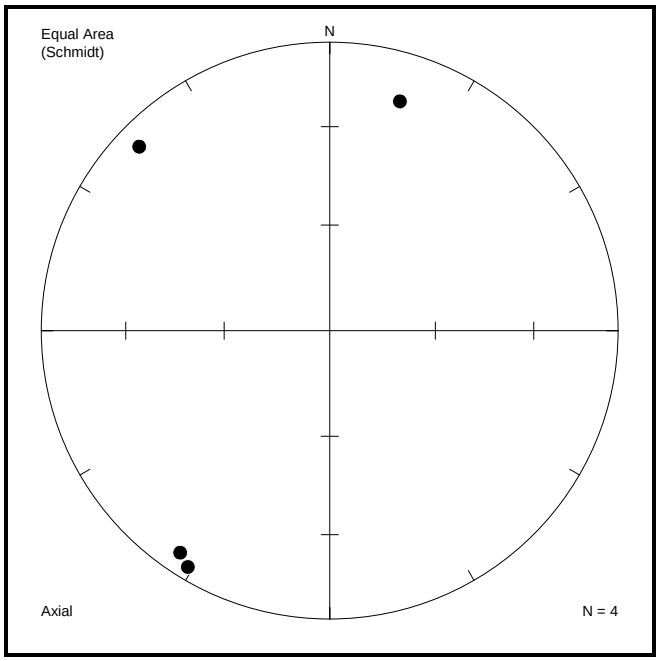

Figure 73: A summary of the poles to joint planes found in block S23° 20' E30° 20'.

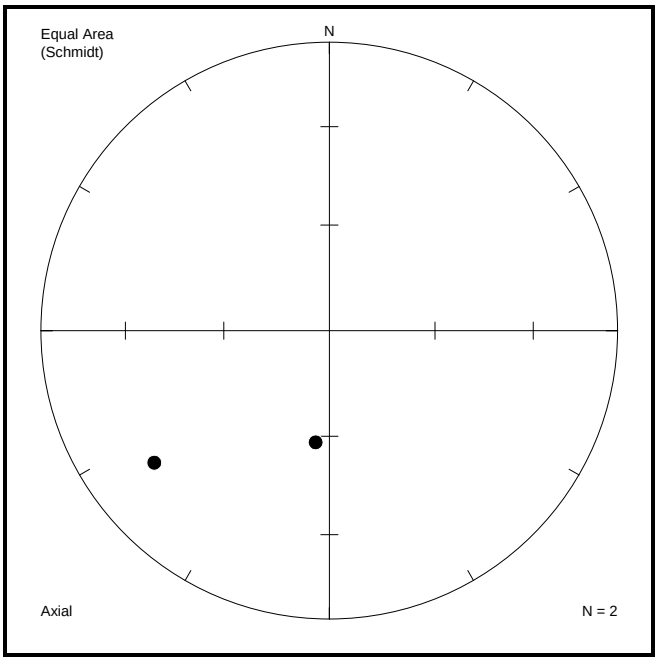

Figure 74: A summary of the poles to joint planes found in block S23° 20' E30° 30'.

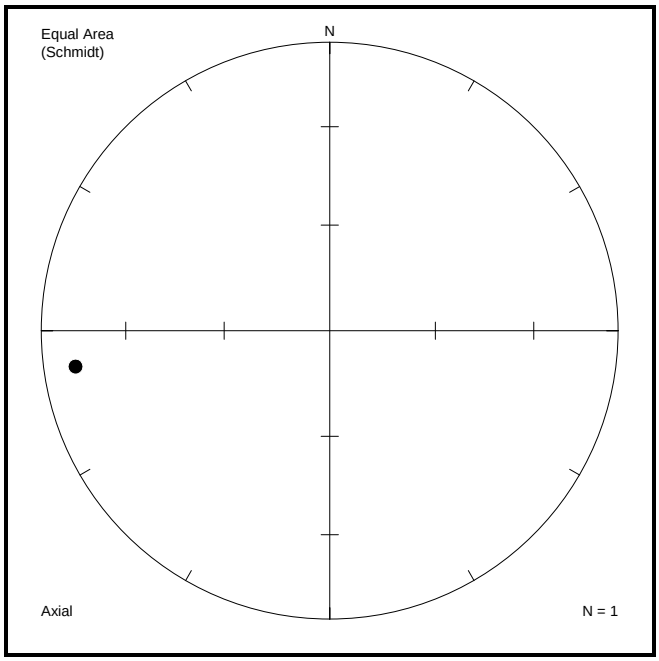

Figure 75: A summary of the poles to joint planes found in block S23° 30' E28° 40'.

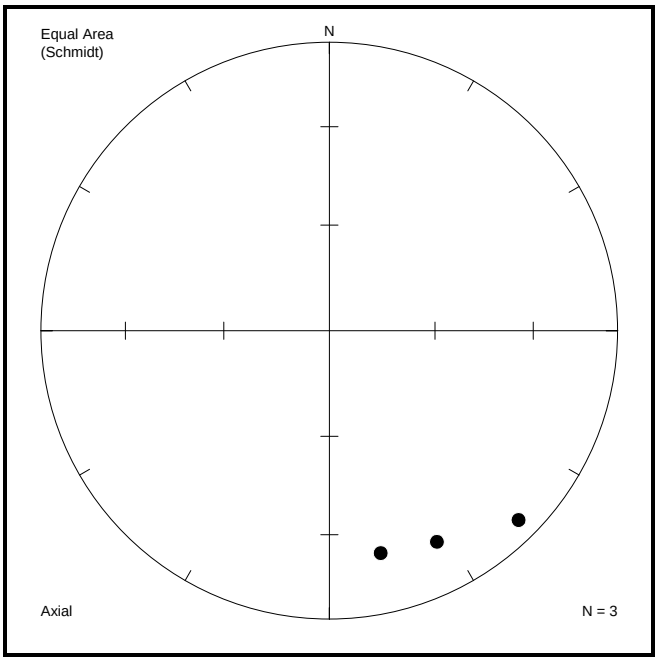

Figure 76: A summary of the poles to joint planes found in block S23° 30' E28° 50'.

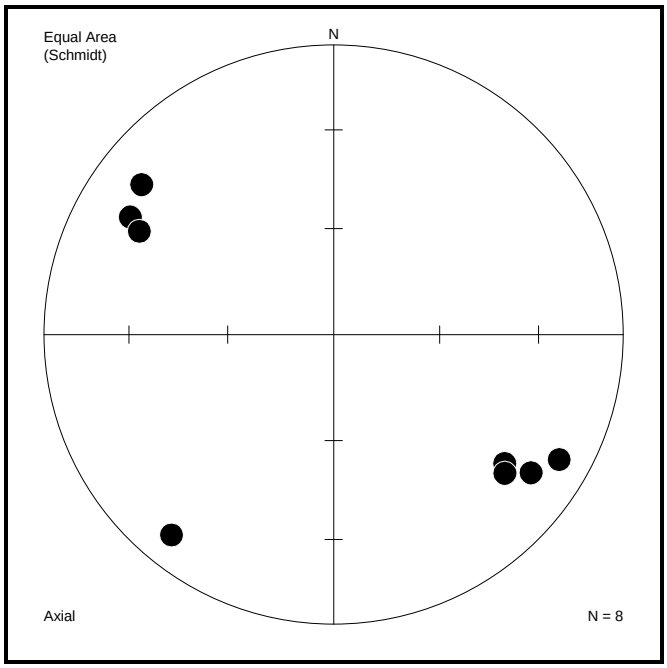

Figure 77: A summary of the poles to joint planes found in block S23° 30' E29° 20'.

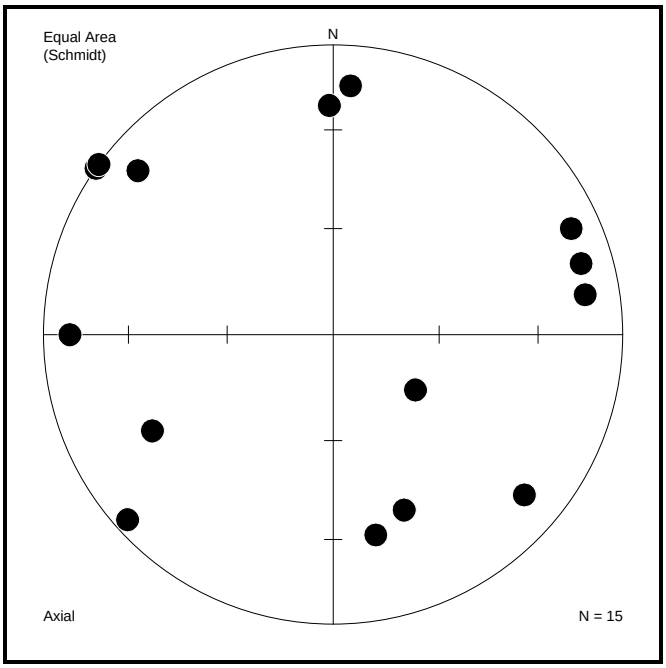

Figure 78: A summary of the poles to joint planes found in block S23° 30' E29° 30'.

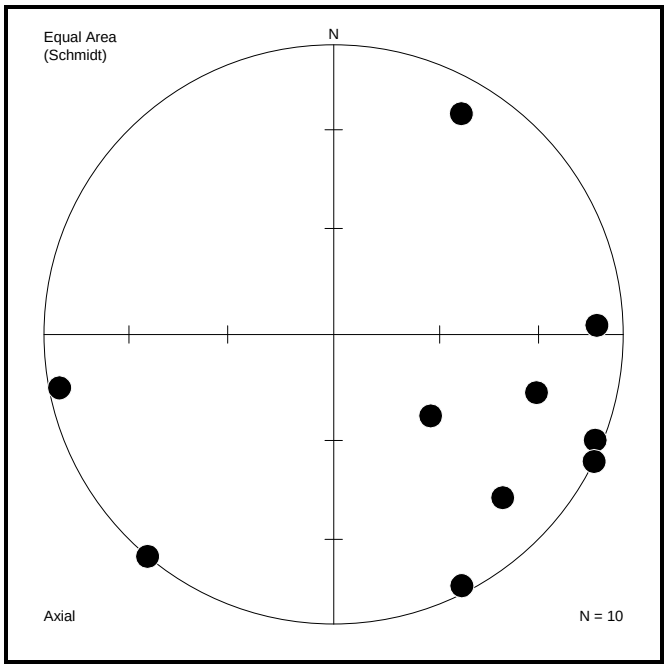

Figure 79: A summary of the poles to joint planes found in block S23° 30' E29° 40'.

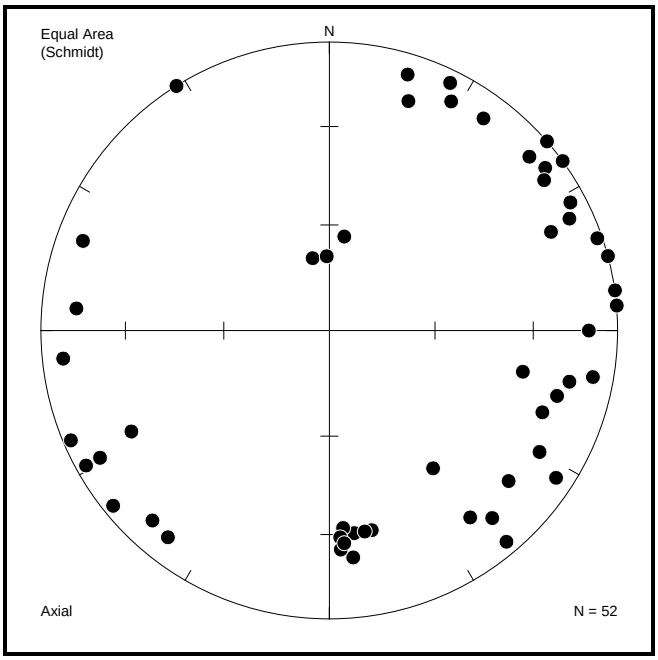

Figure 80: A summary of the poles to joint planes found in block S23° 30' E29° 50'.

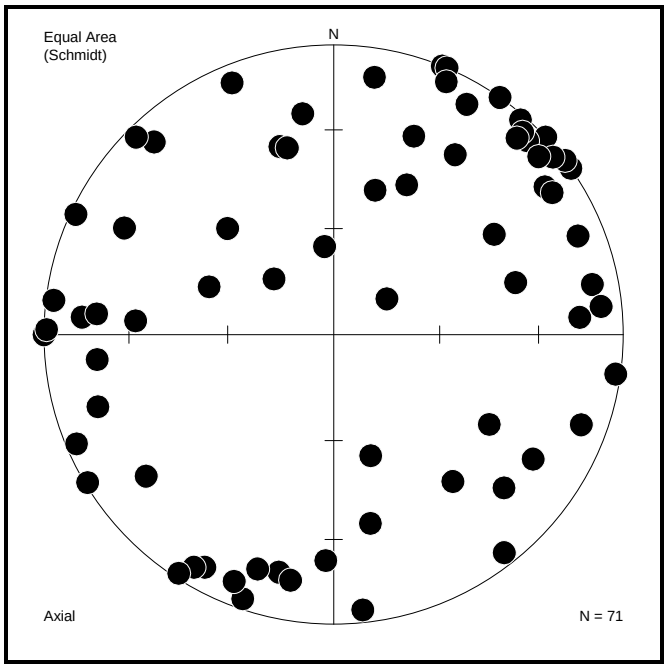

Figure 81: A summary of the poles to joint planes found in block S23° 30' E30° 00'.

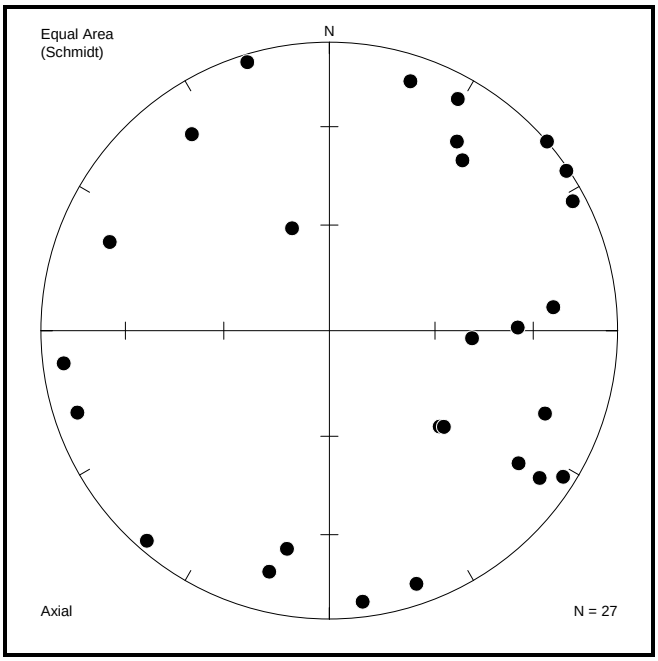

Figure 82: A summary of the poles to joint planes found in block S23° 40' E29° 00'.

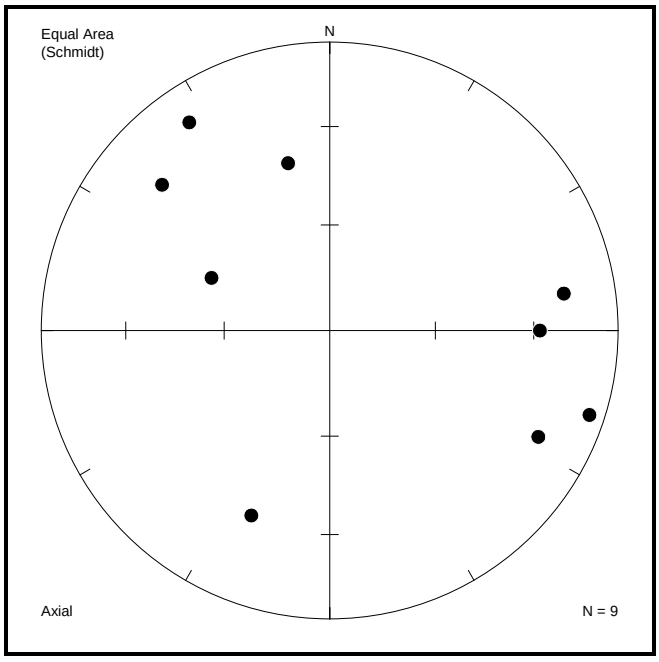

Figure 83: A summary of the poles to joint planes found in block S23° 40' E29° 10'.

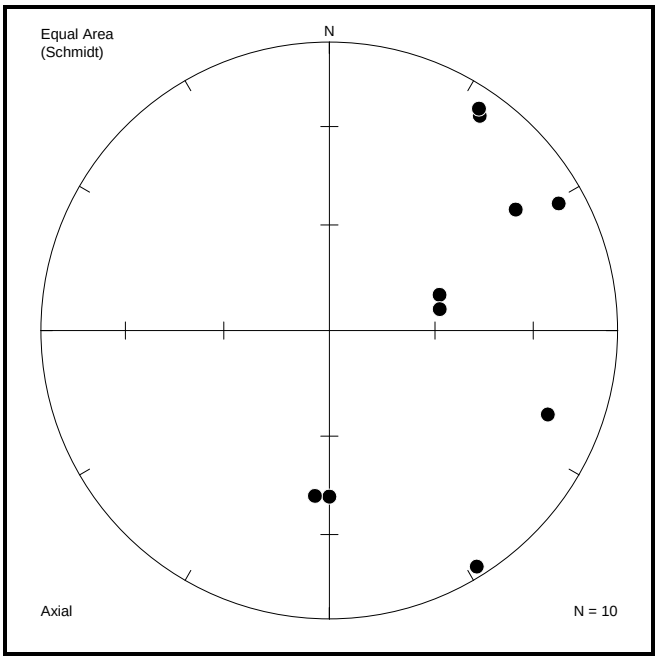

Figure 84: A summary of the poles to joint planes found in block S23° 40' E30° 00'.

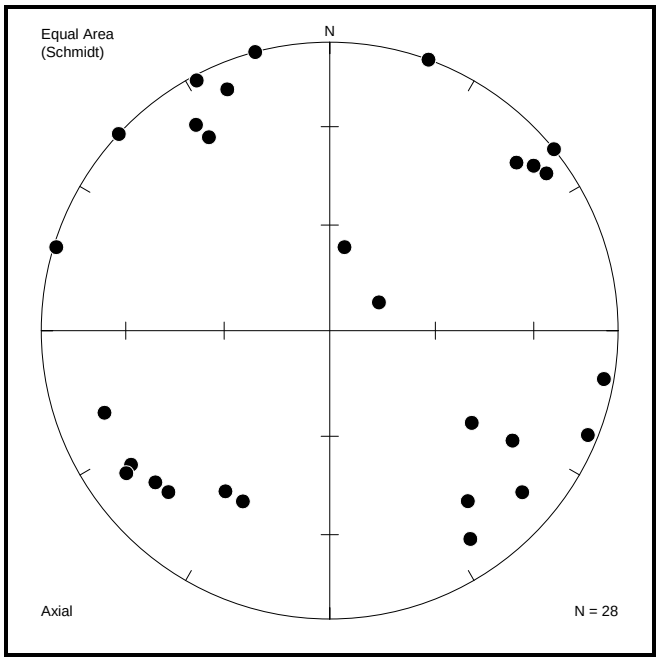

Figure 85: A summary of the poles to joint planes found in block S23° 40' E30° 10'.

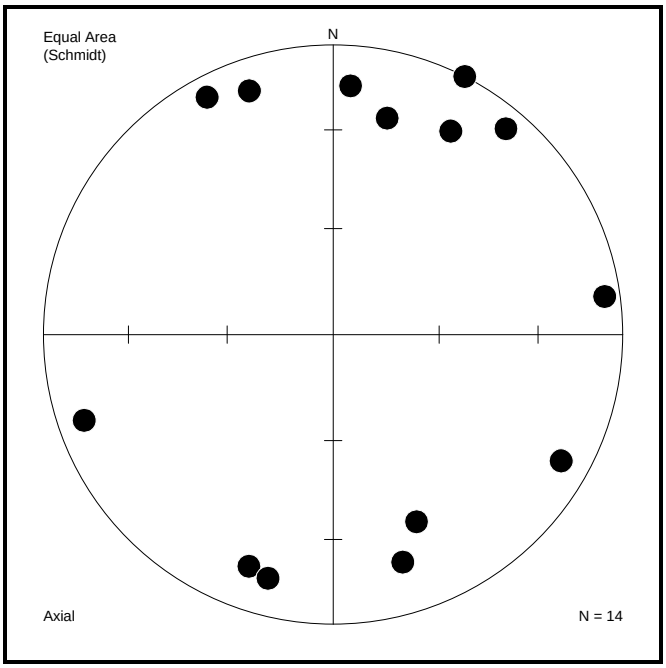

Figure 86: A summary of the poles to joint planes found in block S23° 50' E29° 00'.

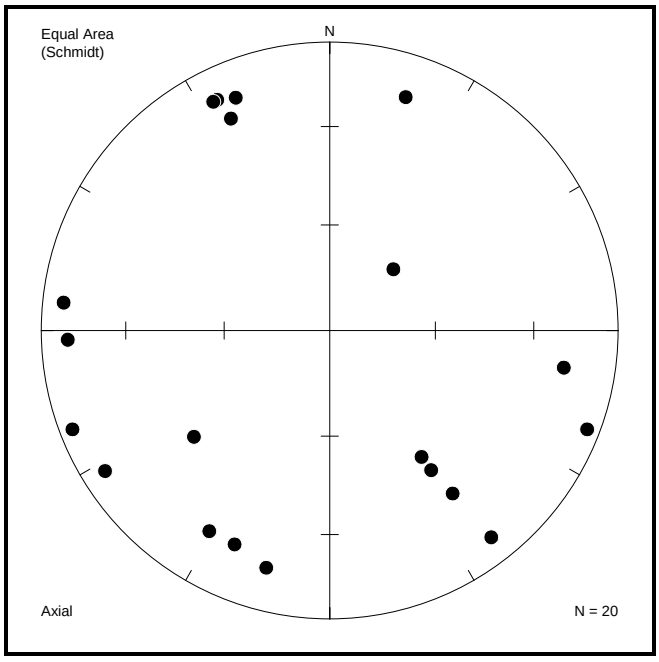

Figure 87: A summary of the poles to joint planes found in block S23° 50' E29° 10'.

iii. Rose diagrams indicating strikes of joints in each 10’ x 10’ block:

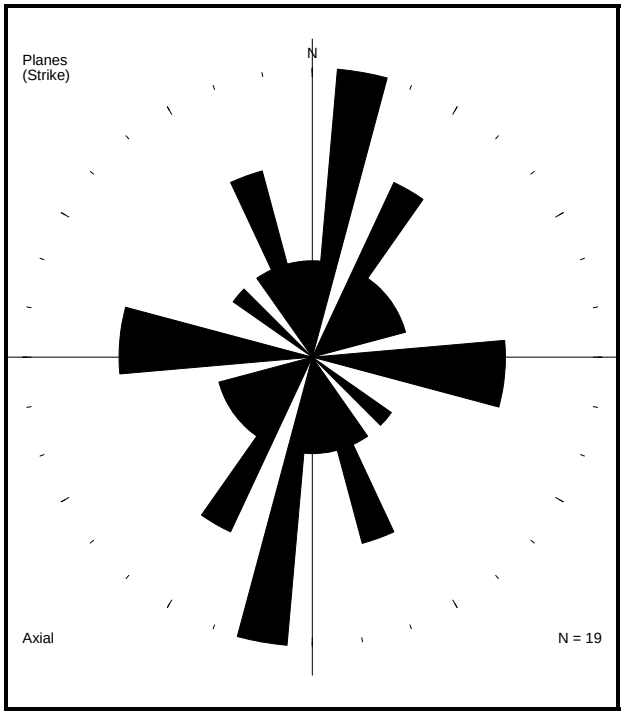

Figure 88: A summary of the joints' strike directions found in block S22° 50’ E29° 50’. (Ten degree intervals centred around 0°)

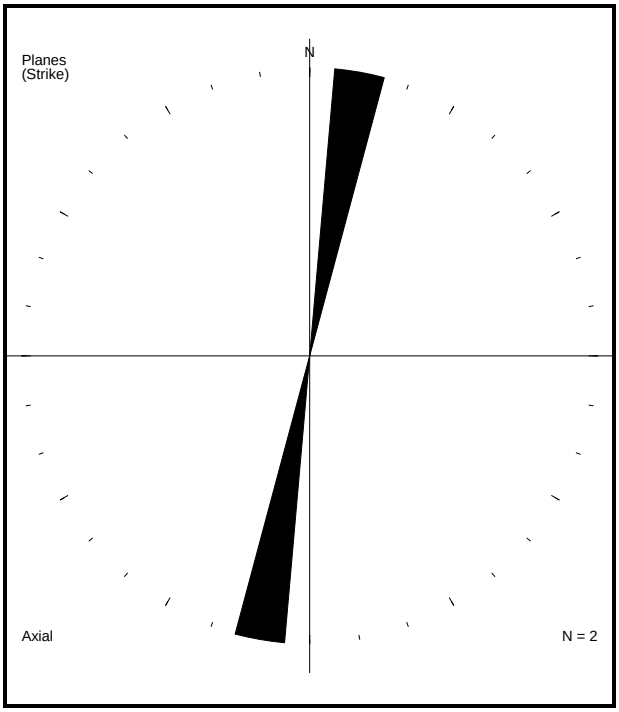

Figure 89: A summary of the joints' strike directions found in block S23° 10’ E29° 00’. (Ten degree intervals centred around 0°)

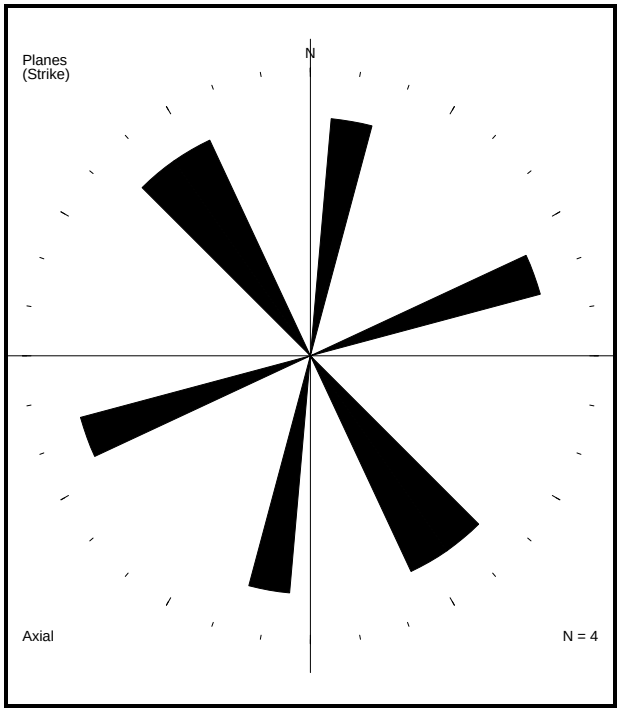

Figure 90: A summary of the joints' strike directions found in block S23° 10’ E29° 30’. (Ten degree intervals centred around 0°)

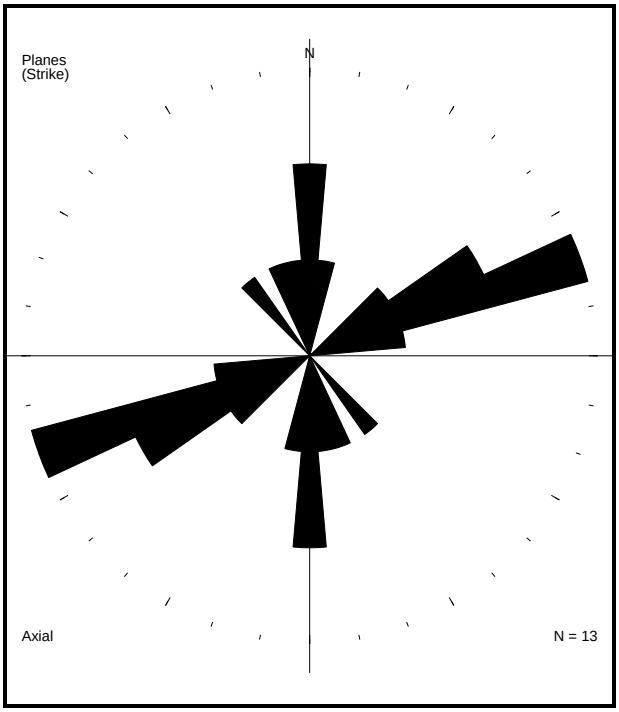

Figure 91: A summary of the joints' strike directions found in block S23° 10’ E30° 00’. (Ten degree intervals centred around 0°)

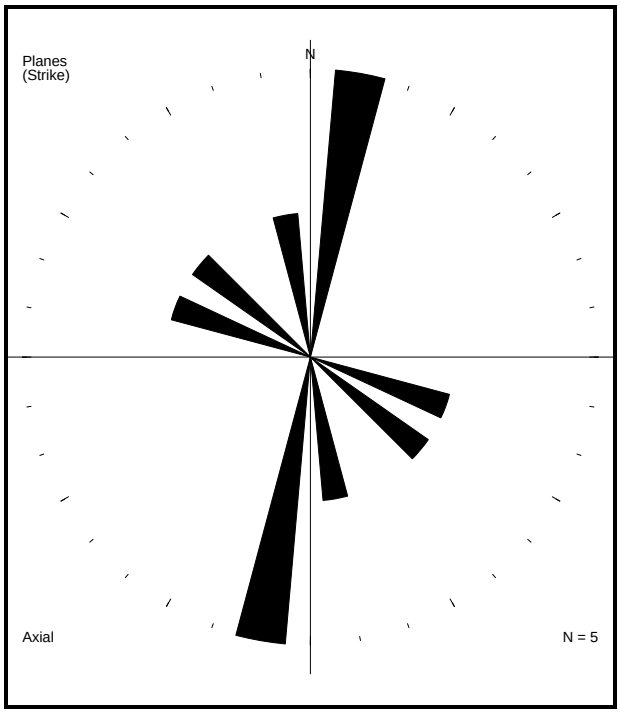

Figure 92: A summary of the joints' strike directions found in block S23° 20' E28° 50'. (Ten degree intervals centred around 0°)

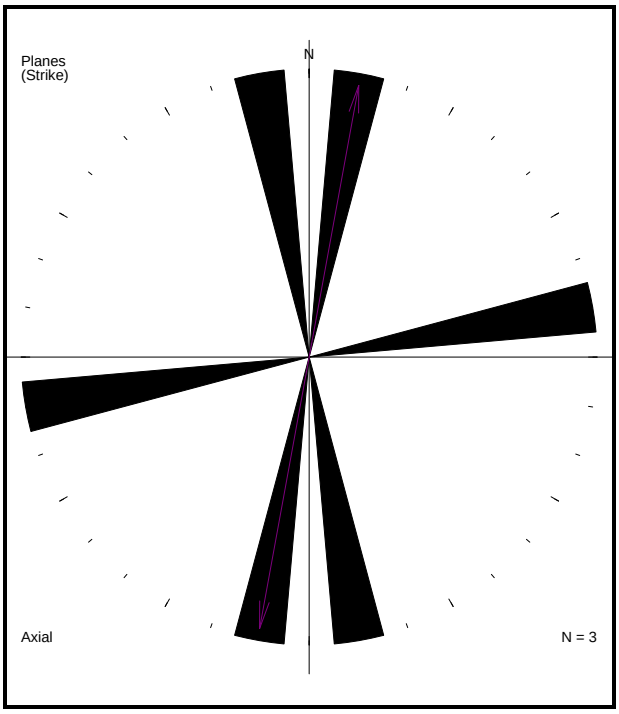

Figure 93: A summary of the joints' strike directions found in block S23° 20' E29° 00'. (Ten degree intervals centred around 0°)

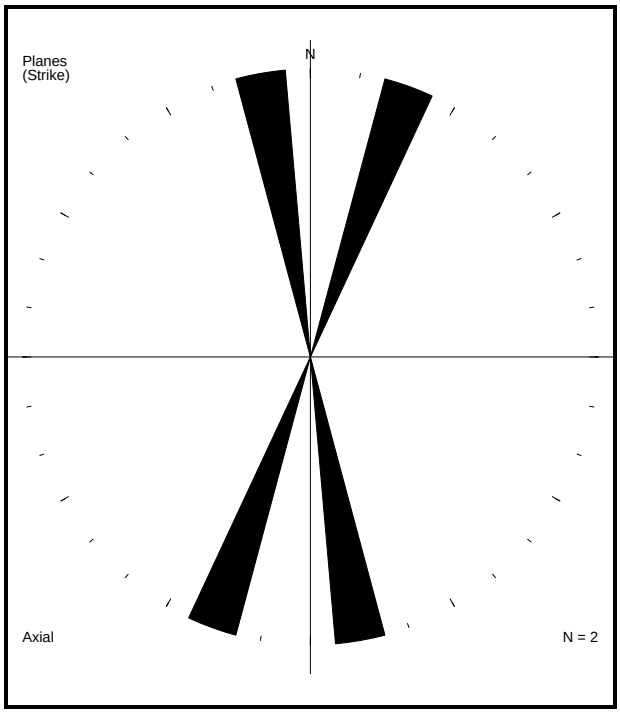

Figure 94: A summary of the joints' strike directions found in block S23° 20' E29° 10'. (Ten degree intervals centred around 0°)

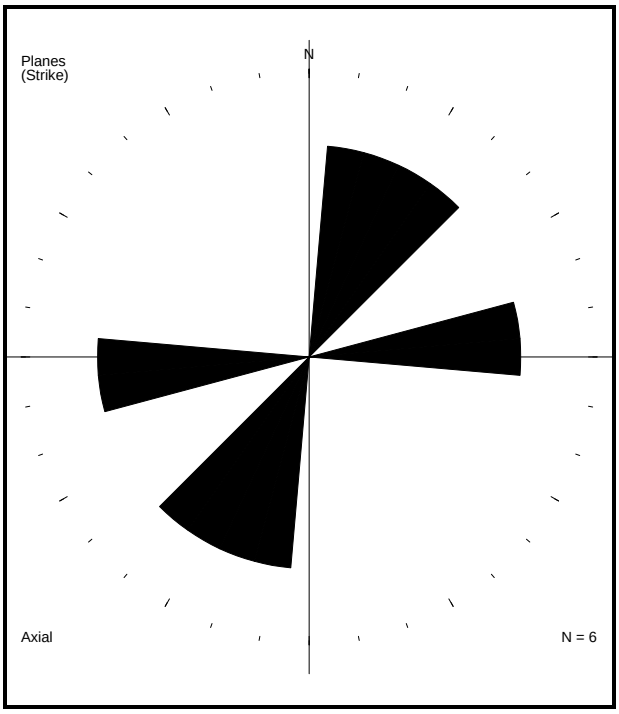

Figure 95: A summary of the joints' strike directions found in block S23° 20' E29° 20'. (Ten degree intervals centred around 0°)

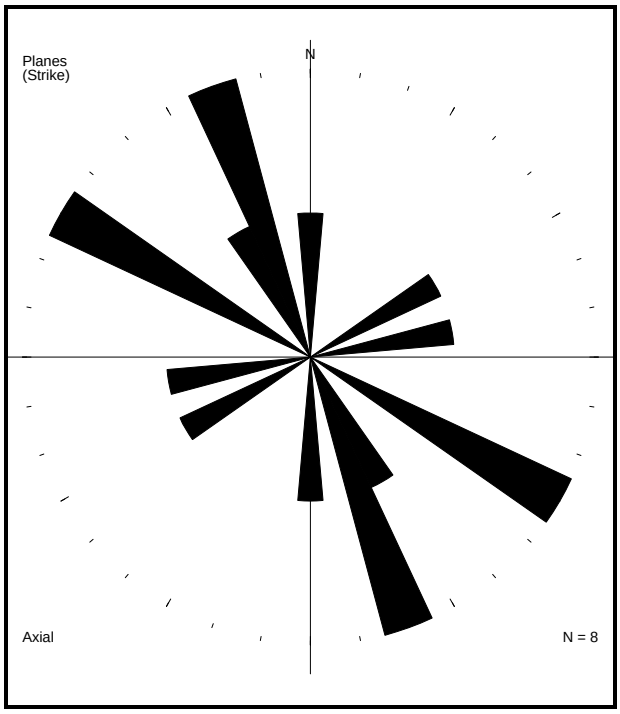

Figure 96: A summary of the joints' strike directions found in block S23° 20' E29° 30'. (Ten degree intervals centred around 0°)

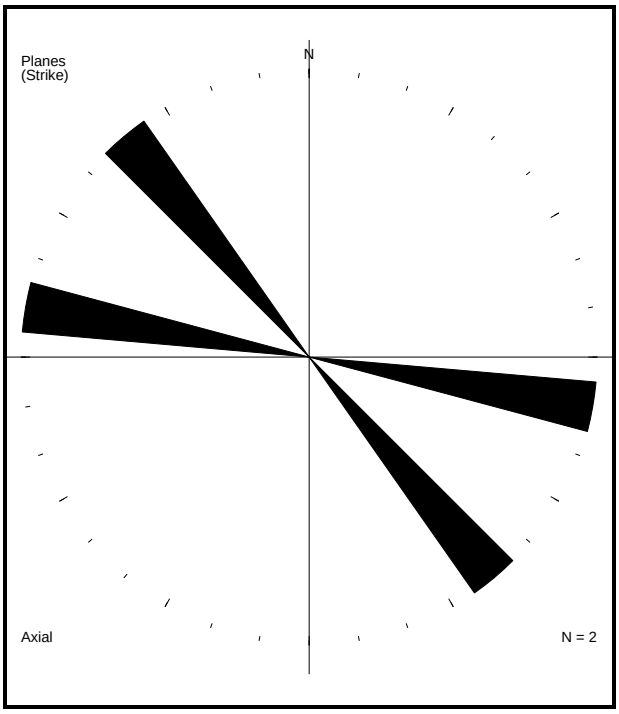

Figure 97: A summary of the joints' strike directions found in block S23° 20' E29° 50'. (Ten degree intervals centred around 0°)

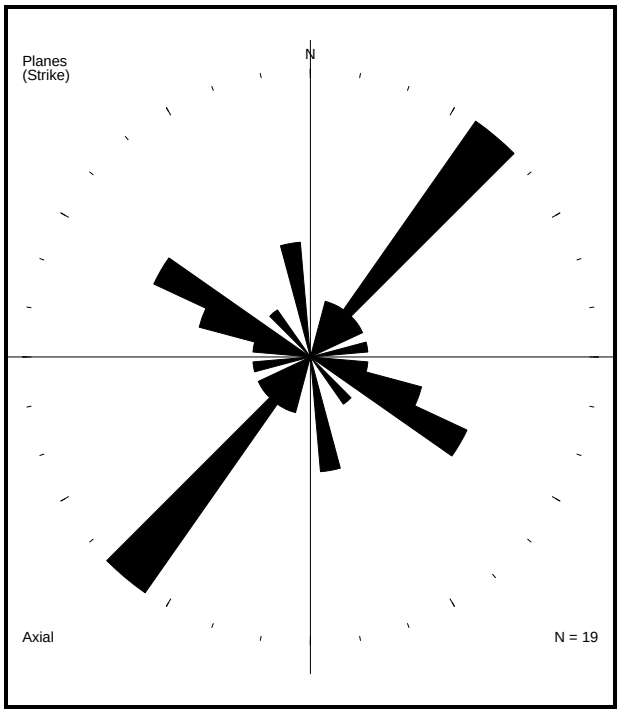

Figure 98: A summary of the joints' strike directions found in block S23° 20' E30° 00'. (Ten degree intervals centred around 0°)

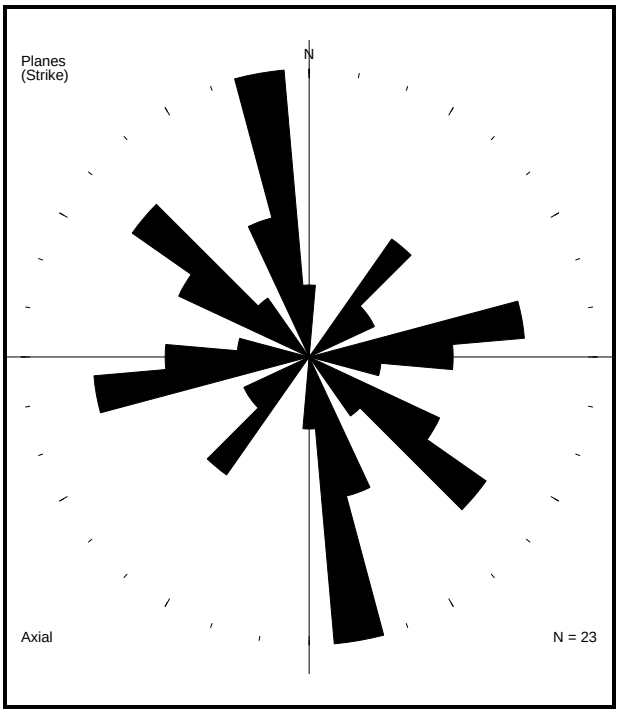

Figure 99: A summary of the joints' strike directions found in block S23° 20' E30° 10'. (Ten degree intervals centred around 0°)

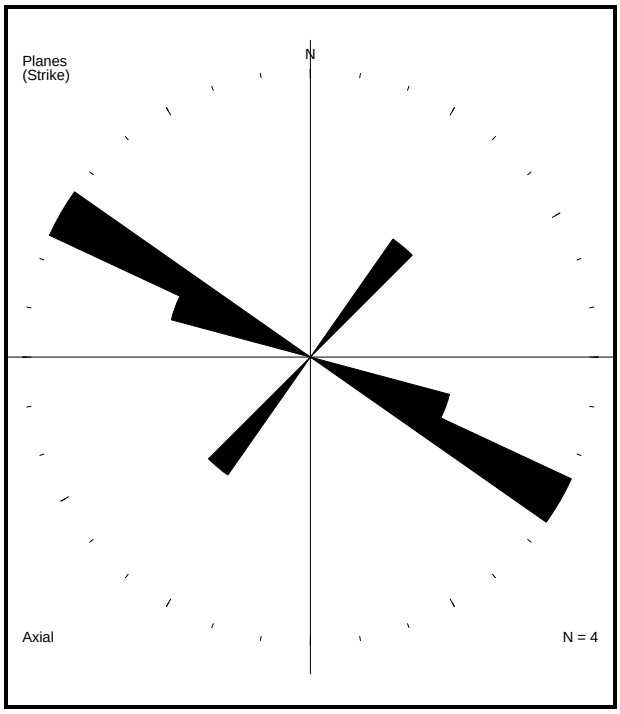

Figure 100: A summary of the joints' strike directions found in block S23° 20' E30° 20'. (Ten degree intervals centred around 0°)

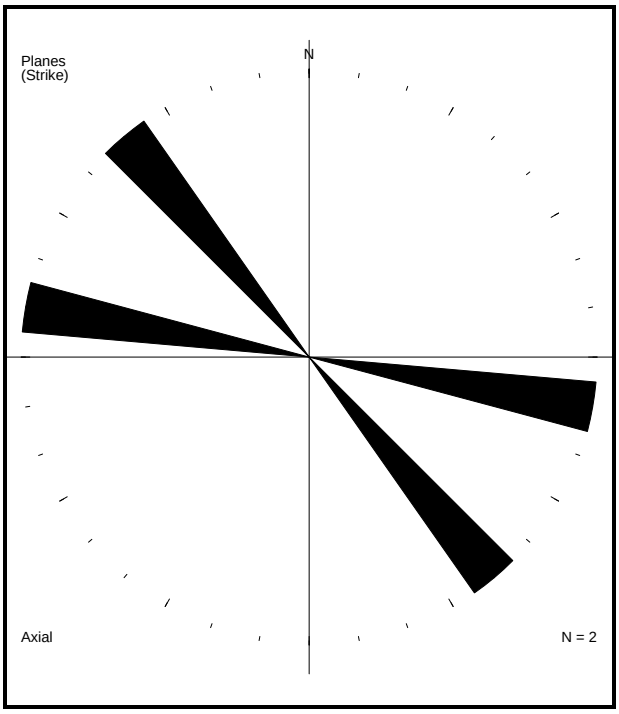

Figure 101: A summary of the joints' strike directions found in block S23° 20' E30° 30'. (Ten degree intervals centred around 0°)

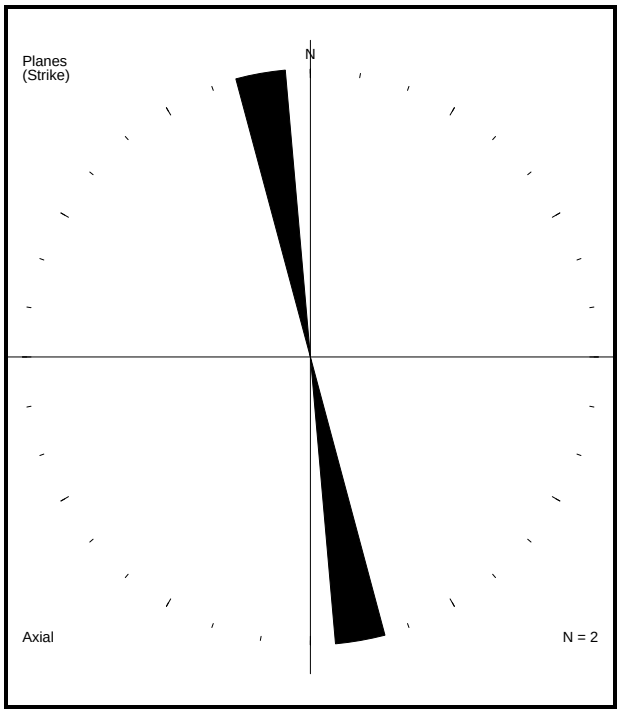

Figure 102: A summary of the joints' strike directions found in block S23° 30' E28° 40'. (Ten degree intervals centred around 0°)

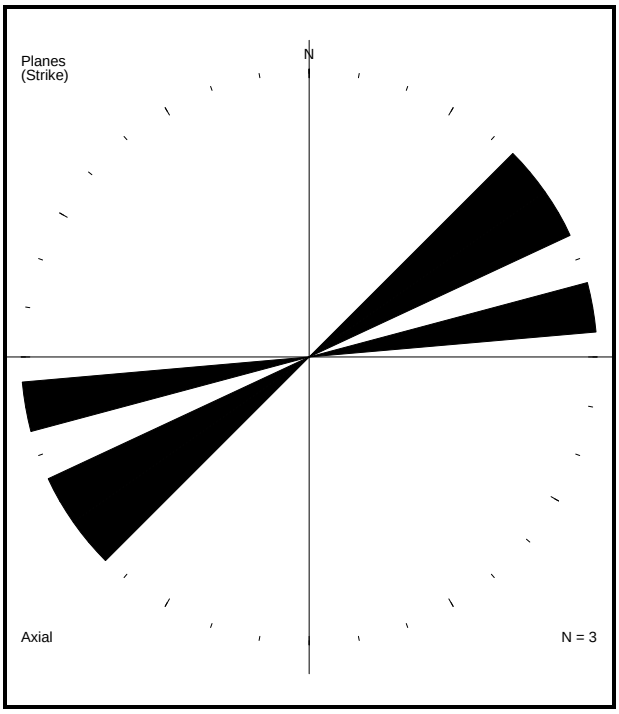

Figure 103: A summary of the joints' strike directions found in block S23° 30' E28° 50'. (Ten degree intervals centred around 0°)

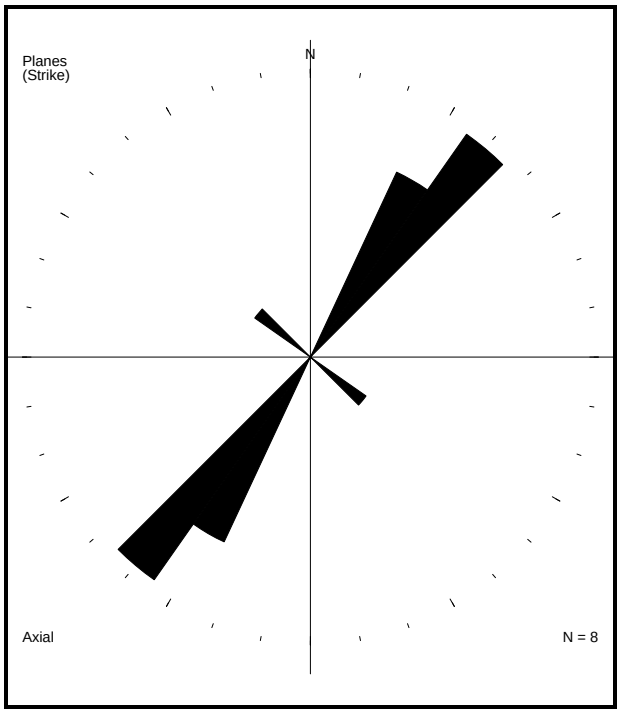

Figure 104: A summary of the joints' strike directions found in block S23° 30' E29° 20'. (Ten degree intervals centred around 0°)

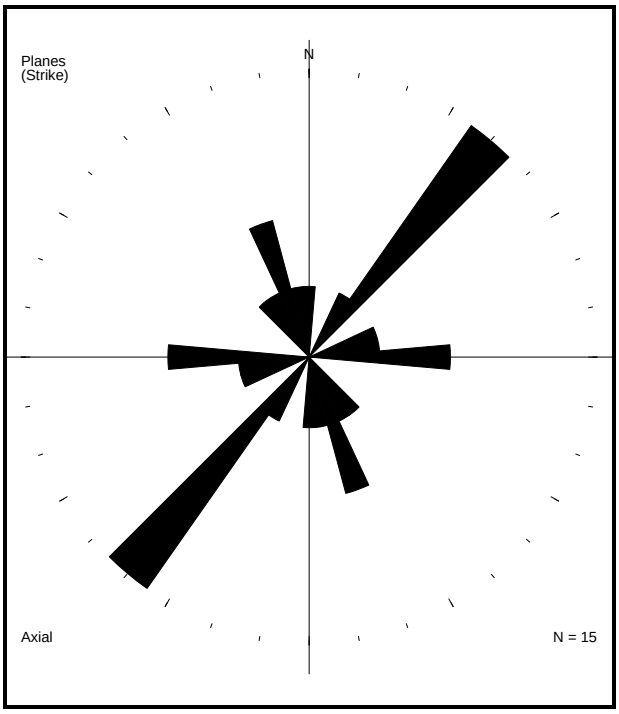

Figure 105: A summary of the joints' strike directions found in block S23° 30' E29° 30'. (Ten degree intervals centred around 0°)

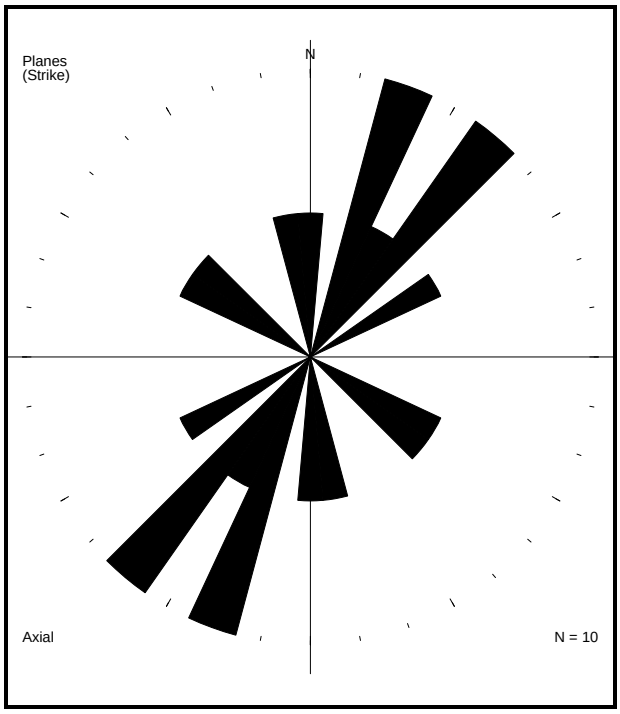

Figure 106: A summary of the joints' strike directions found in block S23° 30' E29° 40'. (Ten degree intervals centred around 0°)

Figure 107: A summary of the joints' strike directions found in block S23° 30' E29° 50'. (Ten degree intervals centred around 0°)

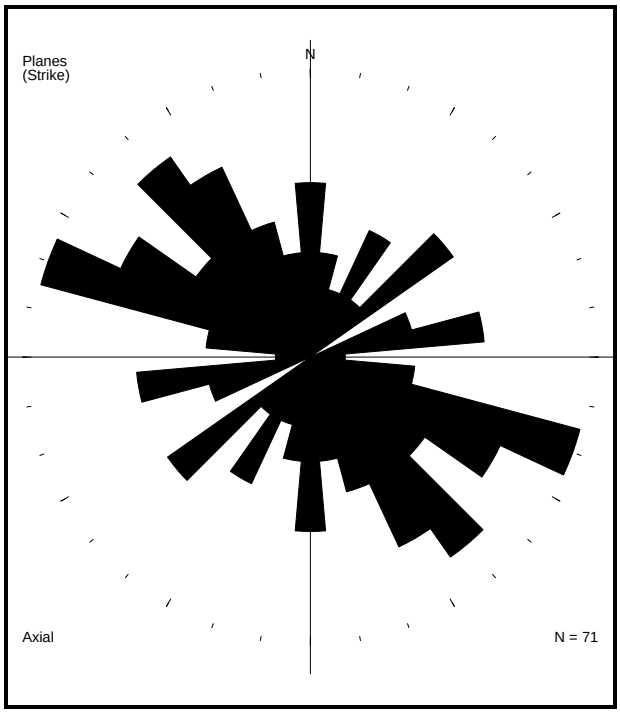

Figure 108: A summary of the joints' strike directions found in block S23° 30' E30° 30'. (Ten degree intervals centred around 0°)

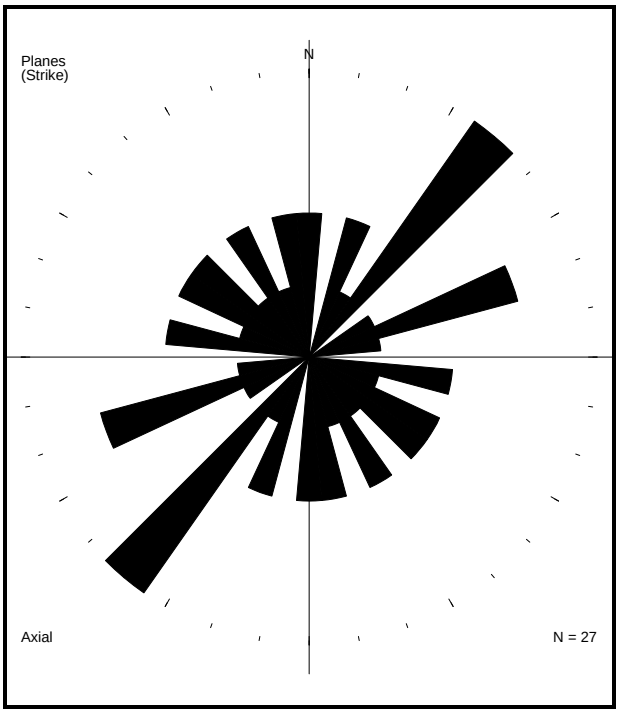

Figure 109: A summary of the joints' strike directions found in block S23° 40' E29° 00'. (Ten degree intervals centred around 0°)

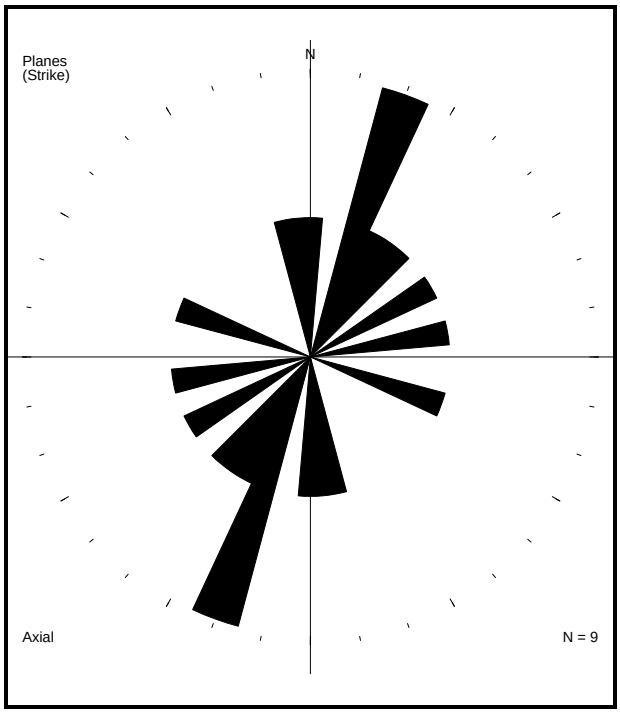

Figure 110: A summary of the joints' strike directions found in block S23° 40' E29° 10'. (Ten degree intervals centred around 0°)

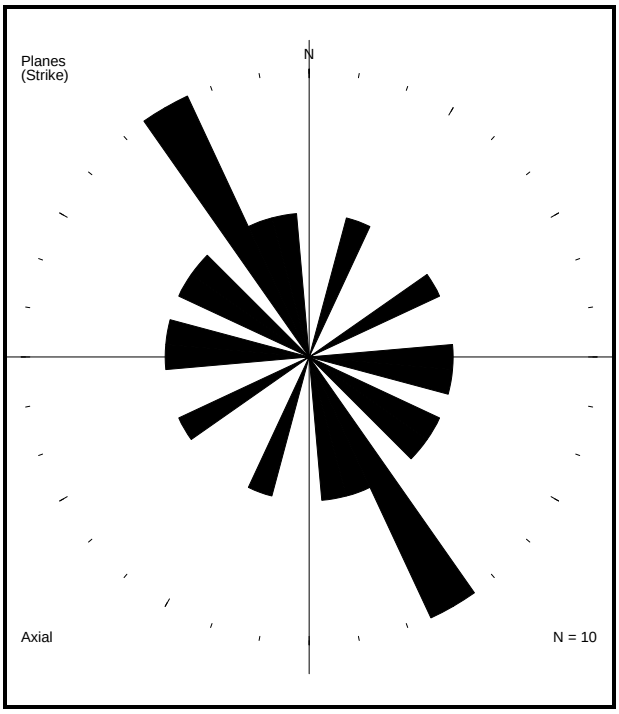

Figure 111: A summary of the joints' strike directions found in block S23° 40' E30° 00'. (Ten degree intervals centred around 0°)

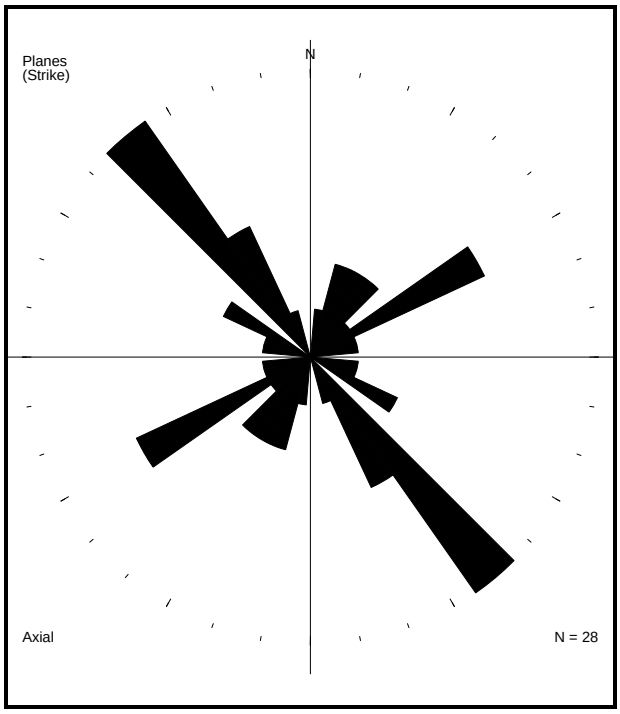

Figure 112: A summary of the joints' strike directions found in block S23° 40' E30° 10'. (Ten degree intervals centred around 0°)

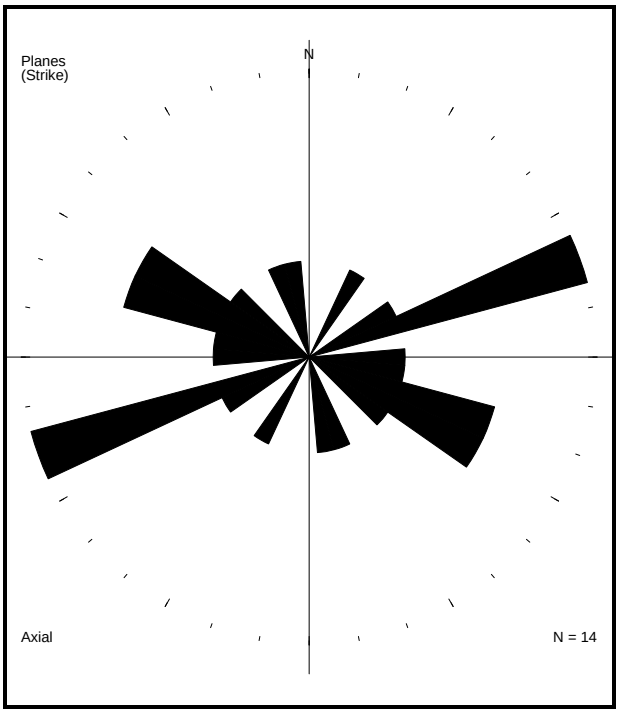

Figure 113: A summary of the joints' strike directions found in block S23° 50' E29° 00'. (Ten degree intervals centred around 0°)

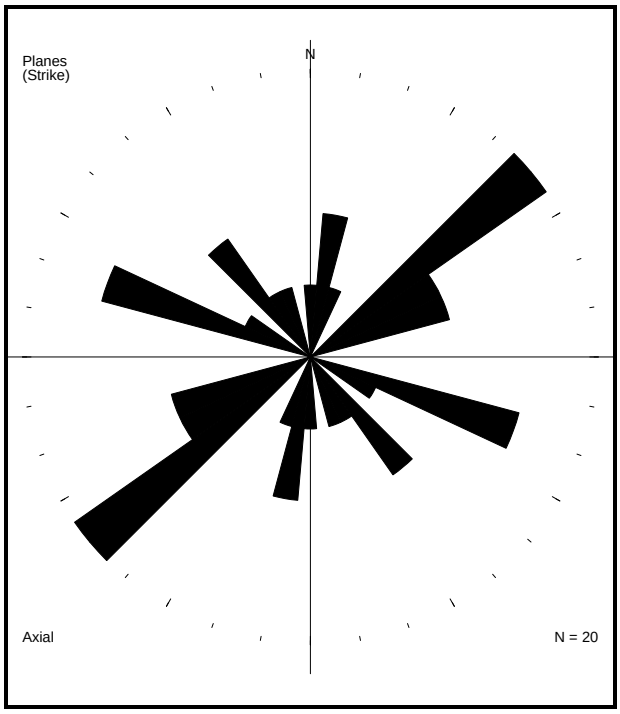

Figure 114: A summary of the joints' strike directions found in block S23° 50' E29° 10'. (Ten degree intervals centred around 0°)

iv. Density distribution intersection lineations of joints in each 10’ x 10’ block (refer to section 4.1):

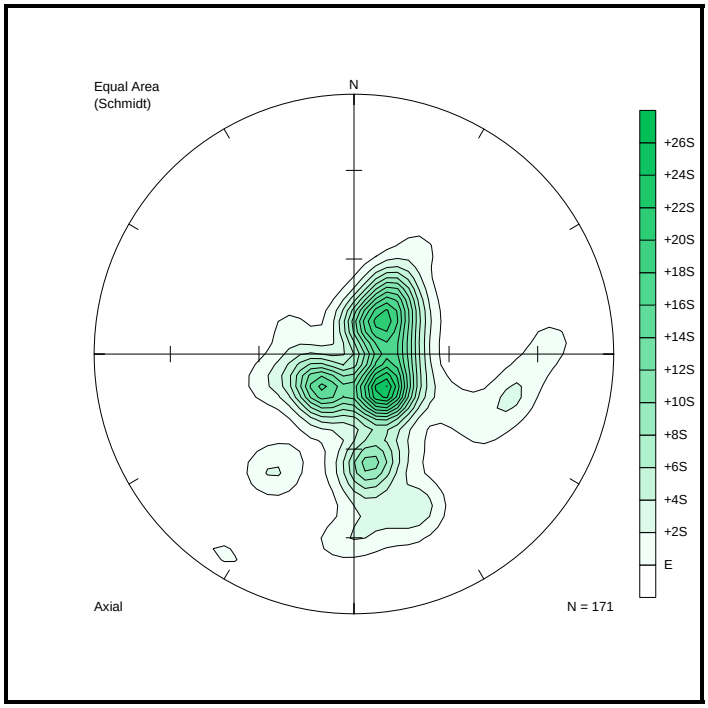

Figure 115: Density distribution of the lineations created by the intercepts of joints in block S22° 50’ E29° 50’.

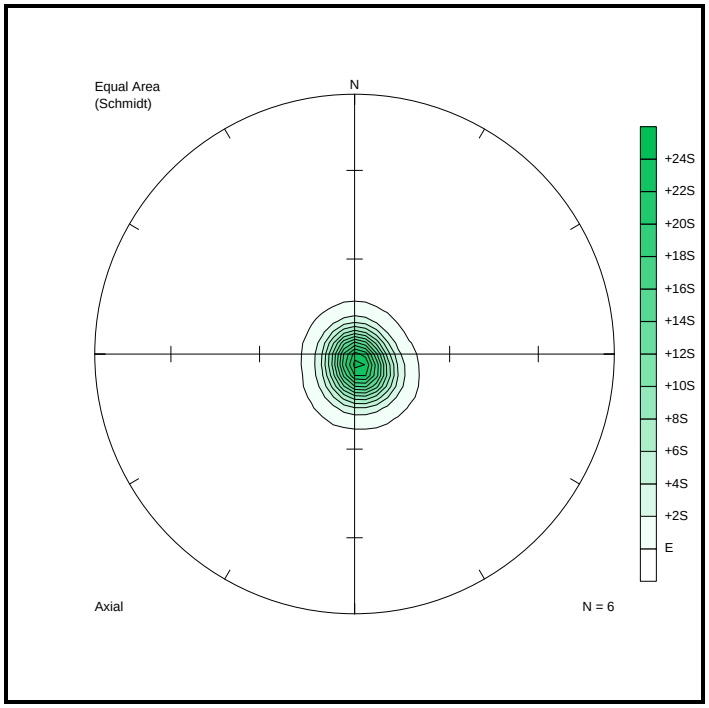

Figure 116: Density distribution of the lineations created by the intercepts of joints in block S23° 10’ E29° 30’.

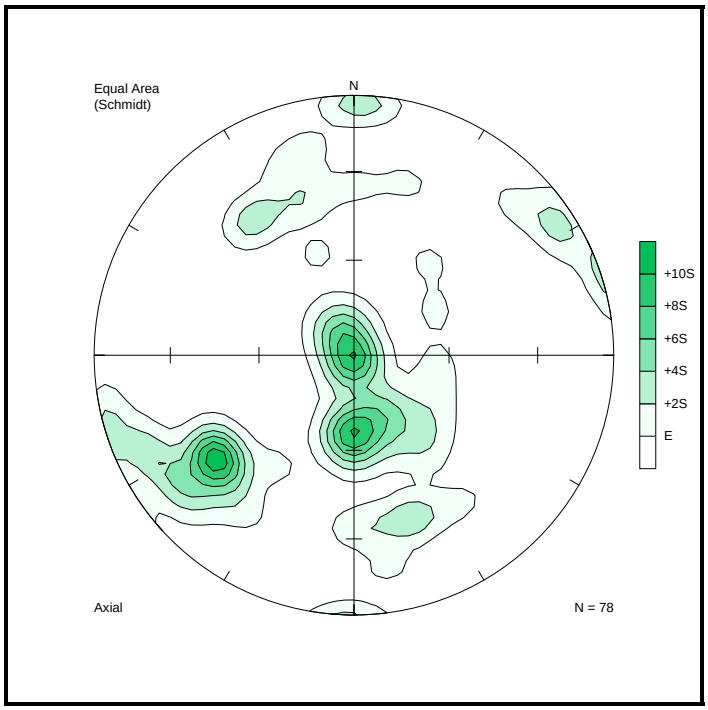

Figure 117: Density distribution of the lineations created by the intercepts of joints in block S23° 10’ E30° 00’.

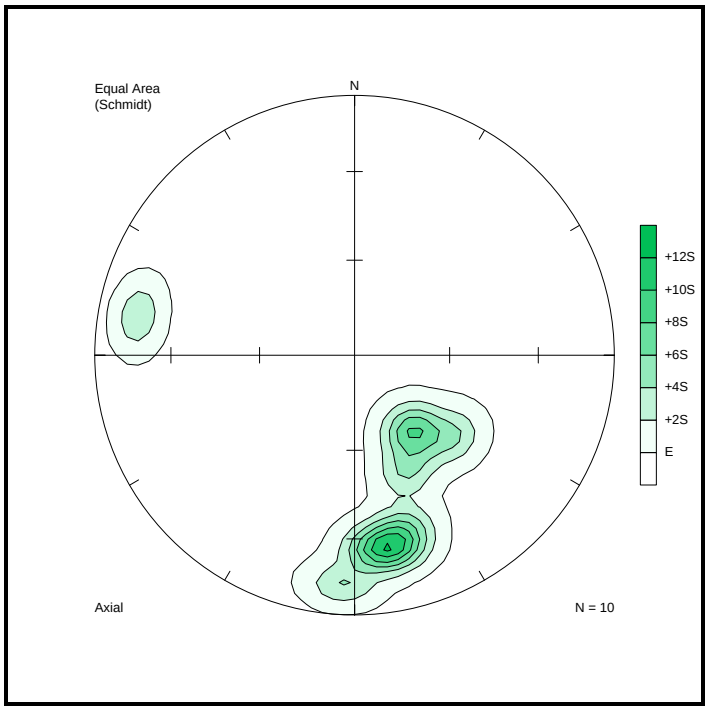

Figure 118: Density distribution of the lineations created by the intercepts of joints in block S23° 20’ E28° 50’.

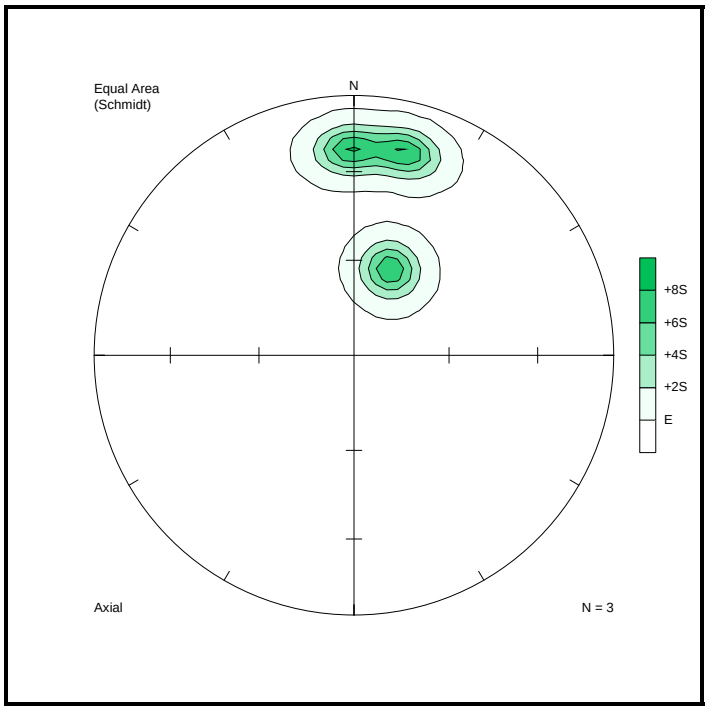

Figure 119: Density distribution of the lineations created by the intercepts of joints in block S23° 20' E29° 00'.

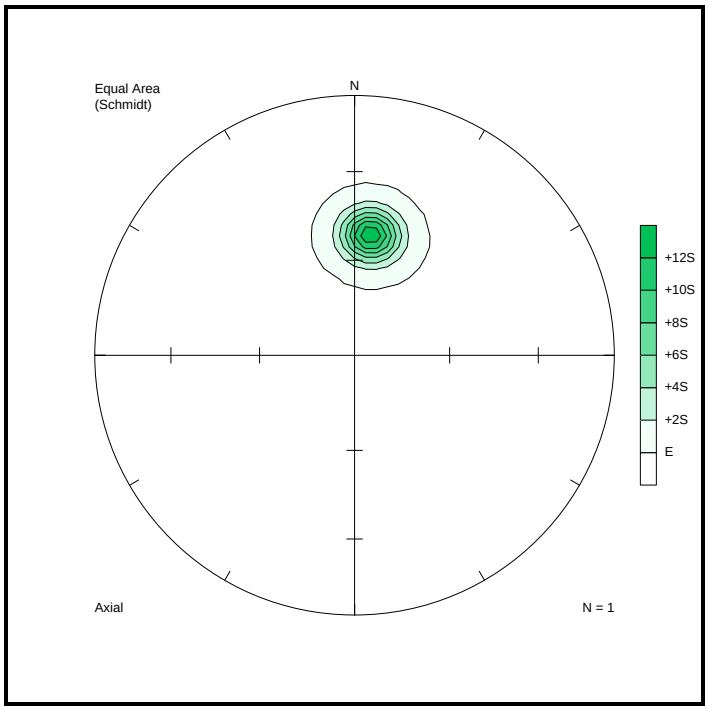

Figure 120: Density distribution of the lineations created by the intercepts of joints in block S23° 20' E29° 10'.

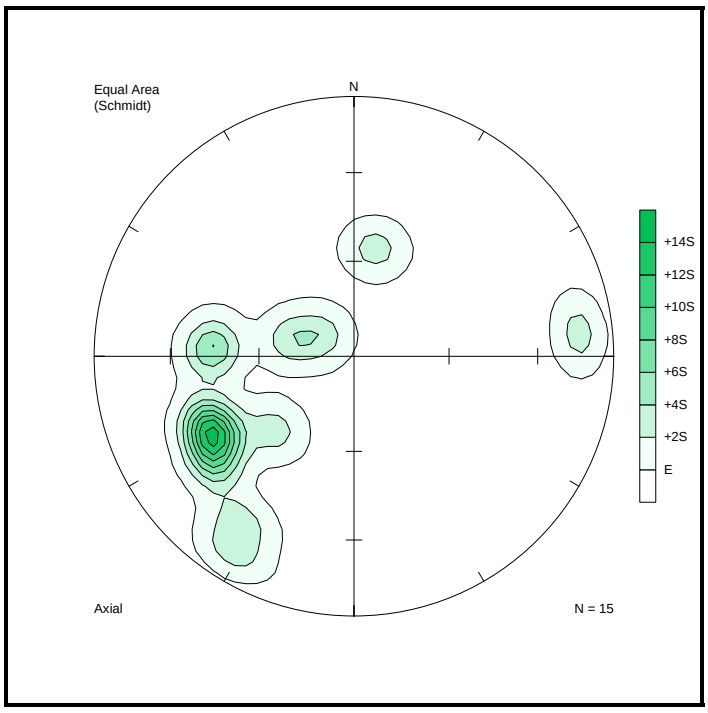

Figure 121: Density distribution of the lineations created by the intercepts of joints in block S23° 20' E29° 20'.

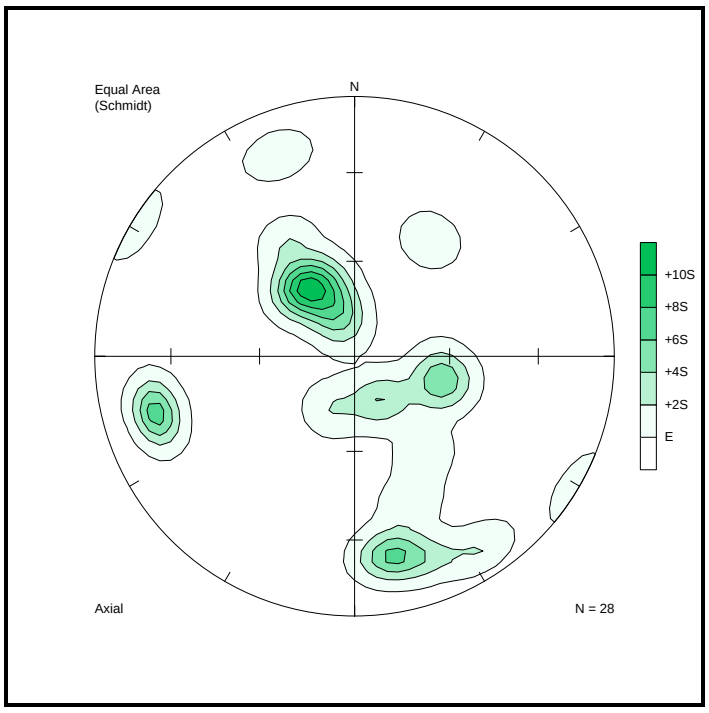

Figure 122: Density distribution of the lineations created by the intercepts of joints in block S23° 20' E29° 30'.

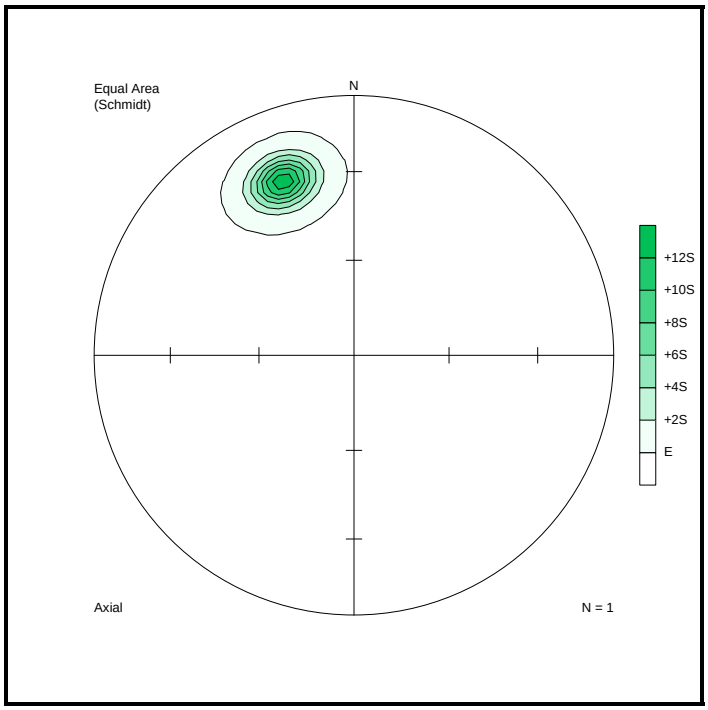

Figure 123: Density distribution of the lineations created by the intercepts of joints in block S23° 20' E29° 50'.

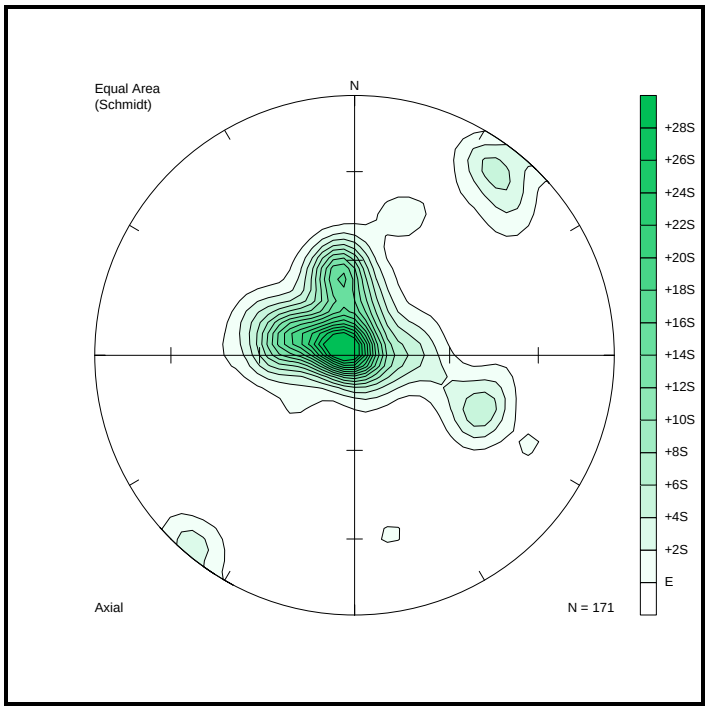

Figure 124: Density distribution of the lineations created by the intercepts of joints in block S23° 20' E30° 00'.

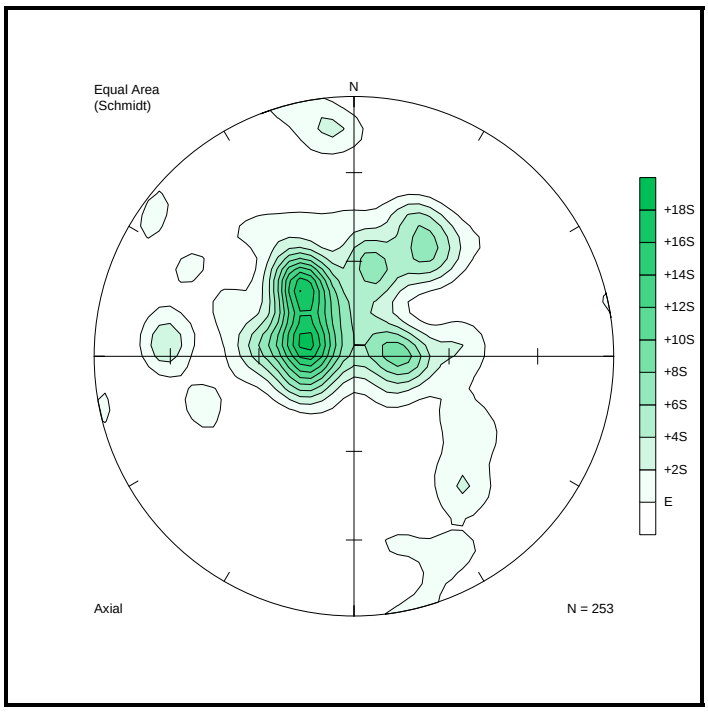

Figure 125: Density distribution of the lineations created by the intercepts of joints in block S23° 20' E30° 10'.

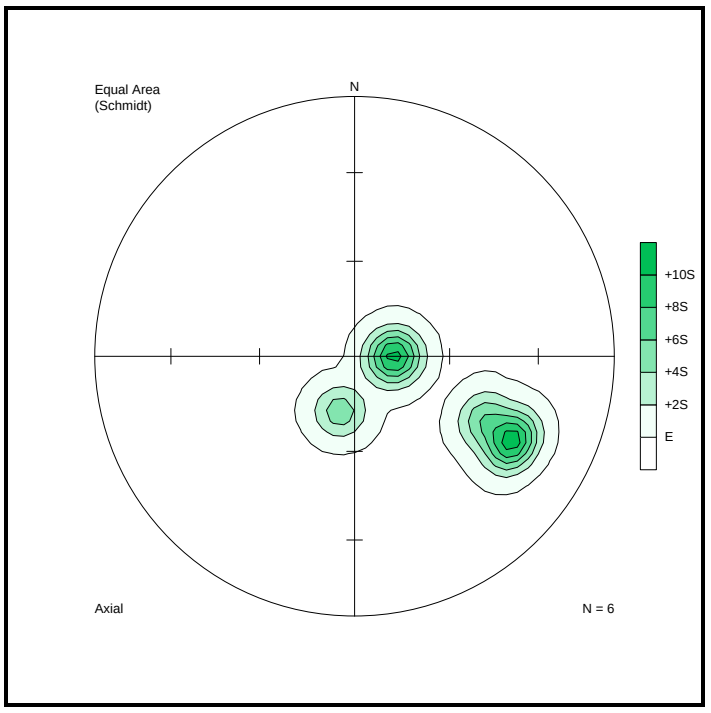

Figure 126: Density distribution of the lineations created by the intercepts of joints in block S23° 20' E30° 20'.

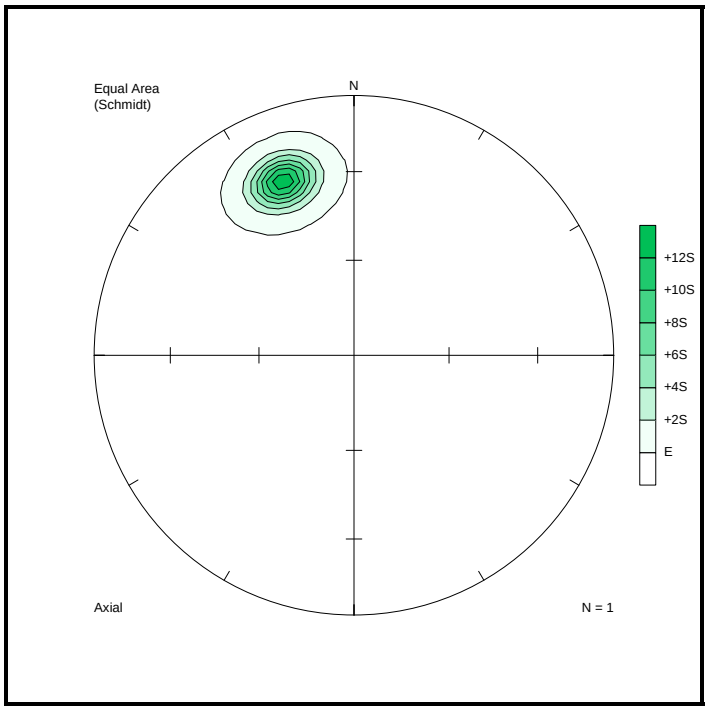

Figure 127: Density distribution of the lineations created by the intercepts of joints in block S23° 20' E30° 30'.

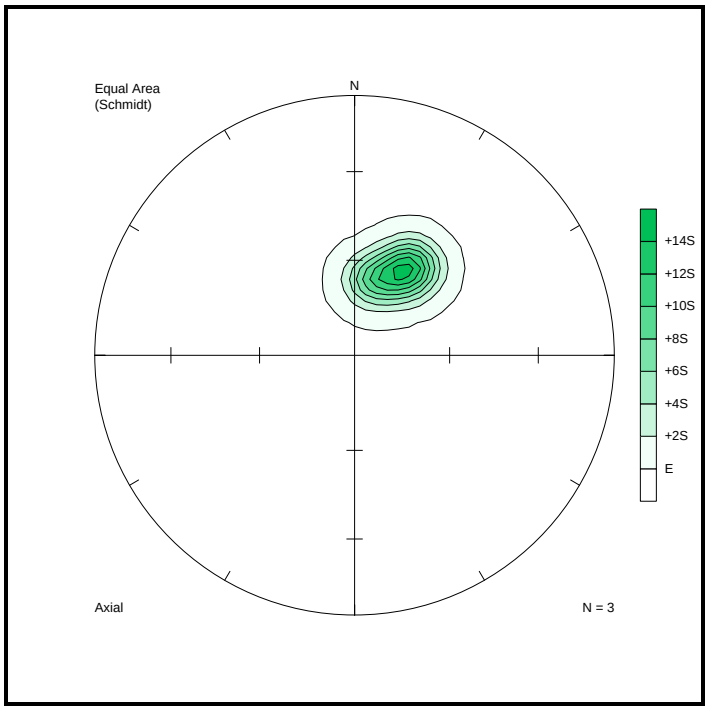

Figure 128: Density distribution of the lineations created by the intercepts of joints in block S23° 30' E28° 50'.

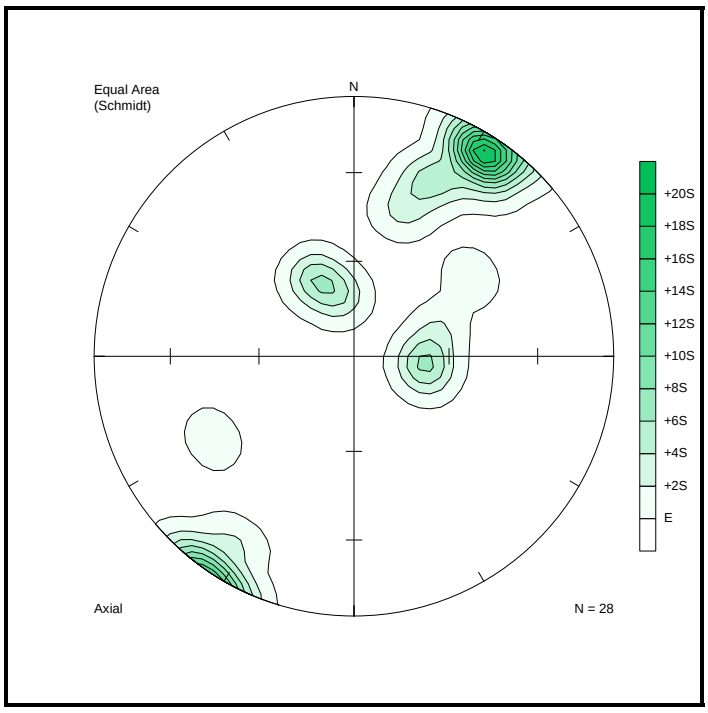

Figure 129: Density distribution of the lineations created by the intercepts of joints in block S23° 30' E29° 20'.

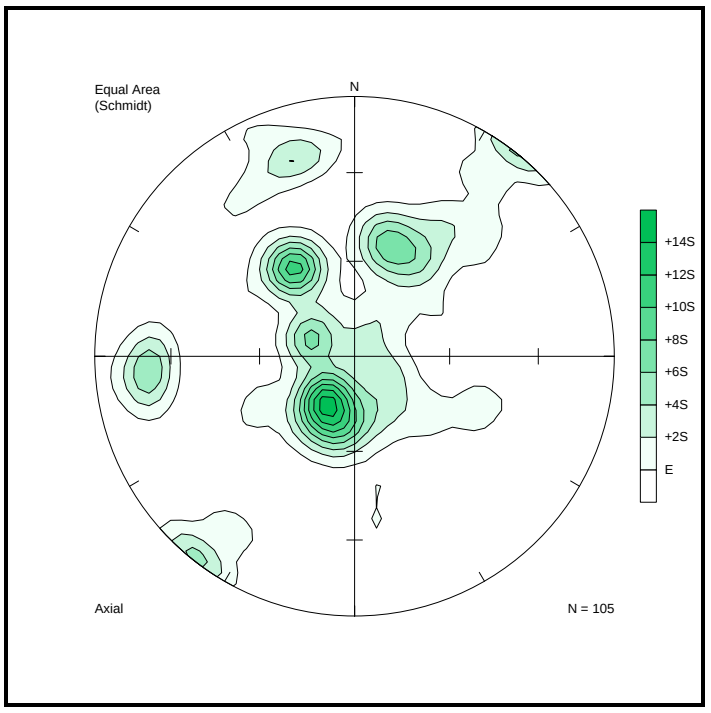

Figure 130: Density distribution of the lineations created by the intercepts of joints in block S23° 30' E29° 30'.

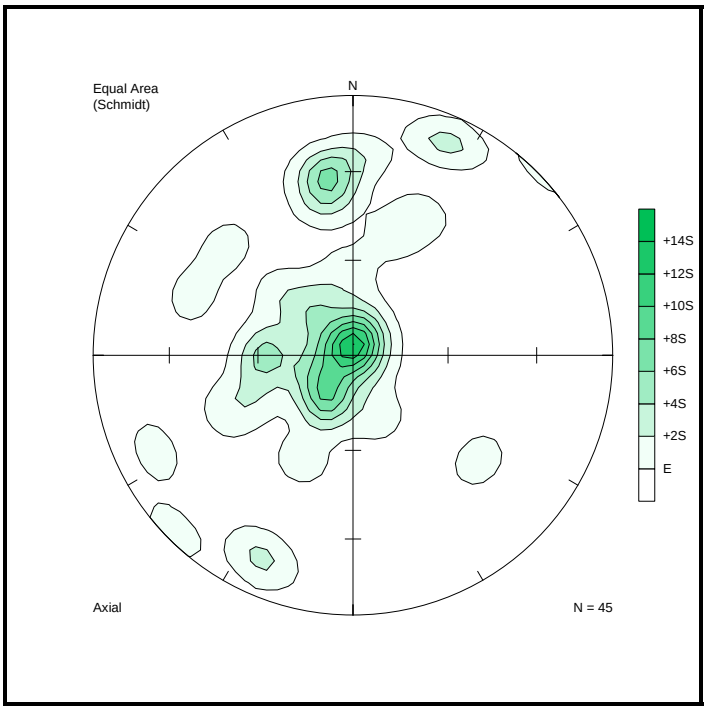

Figure 131: Density distribution of the lineations created by the intercepts of joints in block S23° 30' E29° 40'.

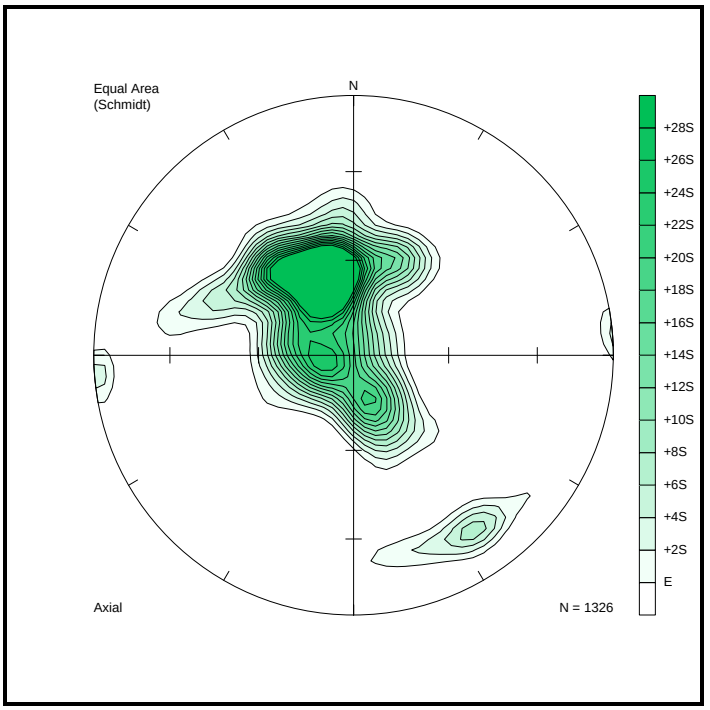

Figure 132: Density distribution of the lineations created by the intercepts of joints in block S23° 30' E29° 50'.

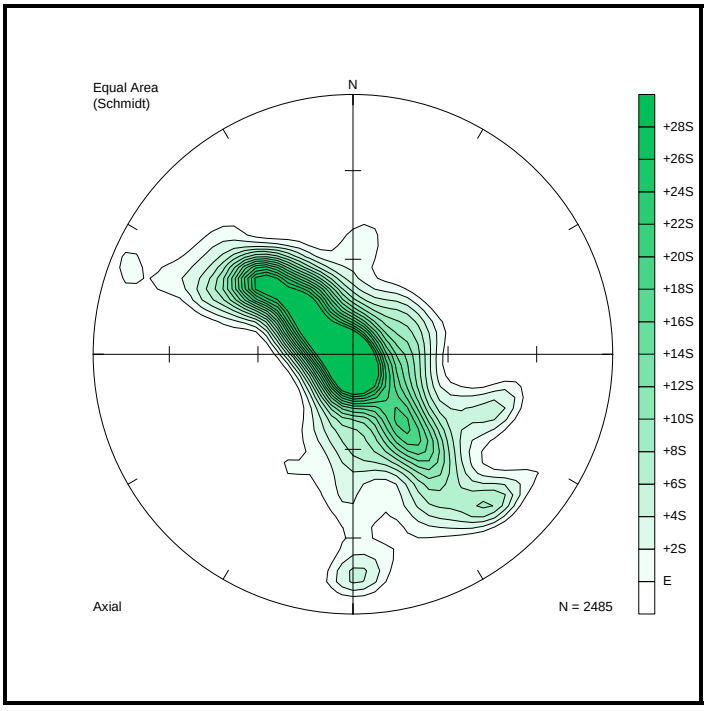

Figure 133: Density distribution of the lineations created by the intercepts of joints in block S23° 30' E30° 00'.

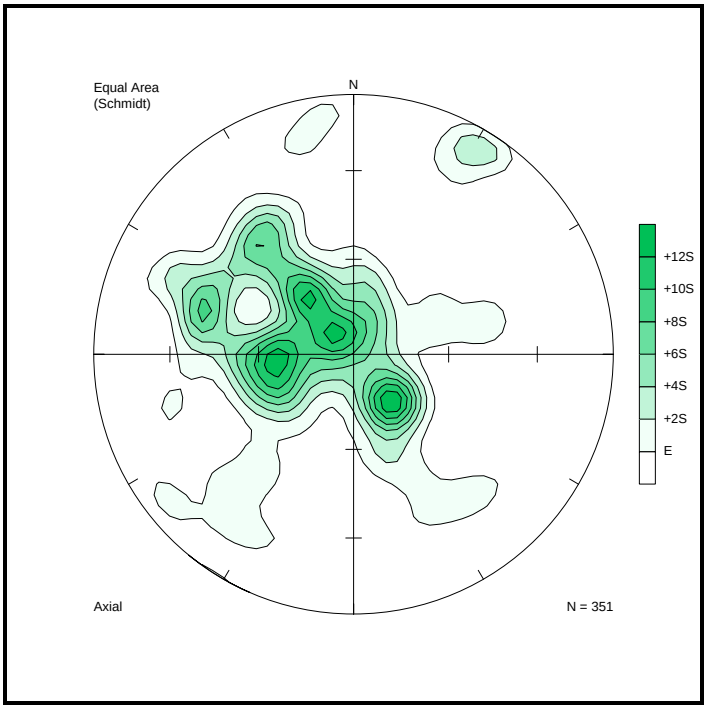

Figure 134: Density distribution of the lineations created by the intercepts of joints in block S23° 40' E29° 00'.

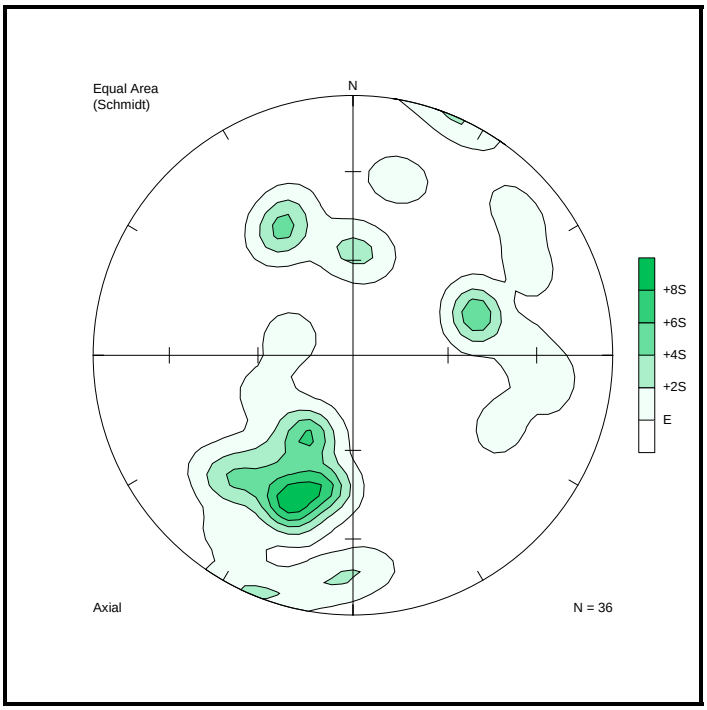

Figure 135: Density distribution of the lineations created by the intercepts of joints in block S23° 40' E29° 10'.

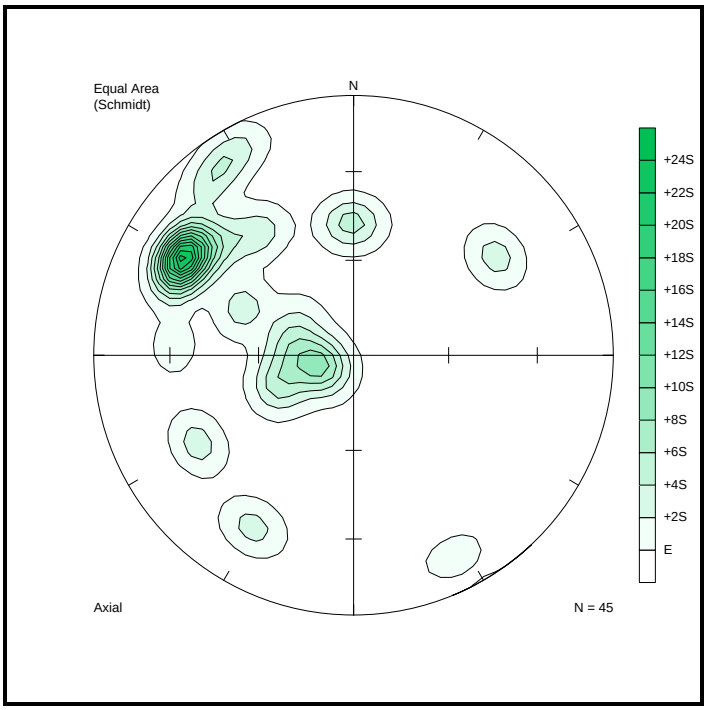

Figure 136: Density distribution of the lineations created by the intercepts of joints in block S23° 40' E30° 00'.

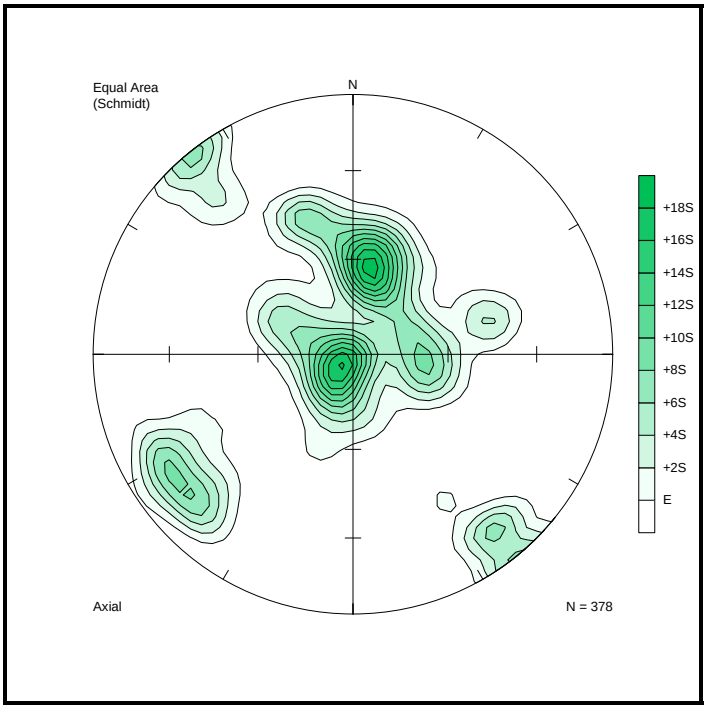

Figure 137: Density distribution of the lineations created by the intercepts of joints in block S23° 40' E30° 10'.

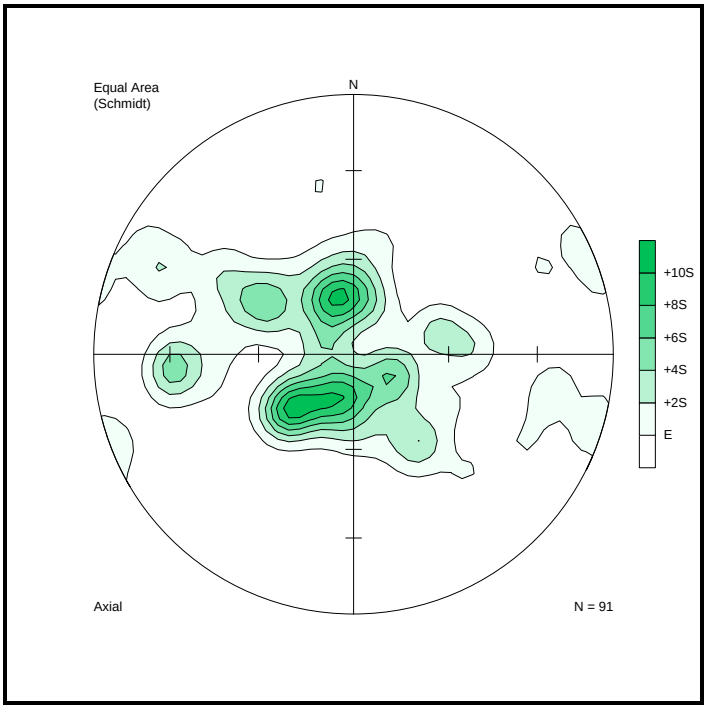

Figure 138: Density distribution of the lineations created by the intercepts of joints in block S23° 50' E29° 00'.

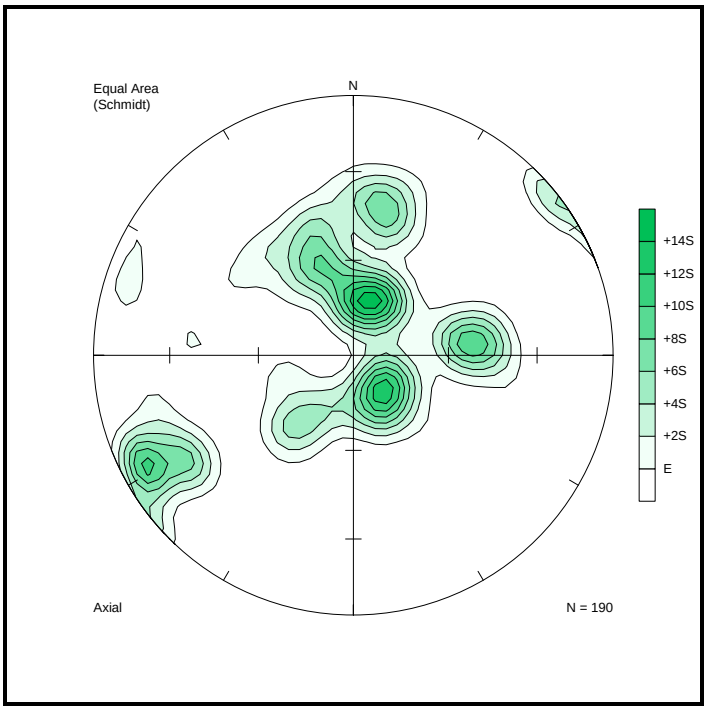

Figure 139: Density distribution of the lineations created by the intercepts of joints in block S23° 50' E29° 10'.

v. An explanation of inverse distance weighting from Wikipedia (Available from: http:/en.wikipedia.org/wiki/Inverse_distance_weighting):

Inverse distance weighting (IDW) is a method for multivariate interpolation, a process of assigning values to unknown points by using values from usually scattered set of known points.

A general form of finding an interpolated value u for a given point $\mathbf{x}$ using IDW is an interpolating function:

$$u(\mathbf{x}) = \frac{\sum_{k=0}^{N} w_k(\mathbf{x}) u_k}{\sum_{k=0}^{N} w_k(\mathbf{x})},$$

where:

$$w_k(\mathbf{x}) = \frac{1}{d(\mathbf{x}, \mathbf{x}_k)^p},$$

is a simple IDW weighting function, as defined by Shepard[1], $\mathbf{x}$ denotes an interpolated (arbitrary) point, $\mathbf{x}_k$ is an interpolating (known) point, d is a given distance (metric operator) from the known point $\mathbf{x}_k$ to the unknown point $\mathbf{x}$, N is the total number of known points used in interpolation and p is a positive real number, called the power parameter. Here weight decreases as distance increases from the interpolated points. Greater values of p assign greater influence to values closest to the interpolated point. For $0 < p < 1$ $u(\mathbf{x})$ has sharp peaks over the interpolated points $\mathbf{x}_k$, while for $p > 1$ the peaks are smooth. The most common value of p is 2.

The *Shepard's method* is a consequence of minimization of a functional related to a measure of deviations between tuples of interpolating points $\{\mathbf{x}, u\}$ and k tuples of interpolated points $\{\mathbf{x}_k, u_k\}$, defined as:

$$\phi(\mathbf{x}, u) = \left(\sum_{k=0}^{N} \frac{(u - u_k)^2}{d(\mathbf{x}, \mathbf{x}_k)^p} \right)^{\frac{1}{p}},$$

derived from the minimizing condition:

$$\frac{\partial \phi(\mathbf{x}, u)}{\partial u} = 0.$$

The method can easily be extended to higher dimensional space and it is in fact a generalization of Lagrange approximation into a multidimensional spaces. A modified version of the algorithm designed for trivariate interpolation was developed by Robert J. Renka and is available in Netlib as algorithm 661 in the Toms Library.